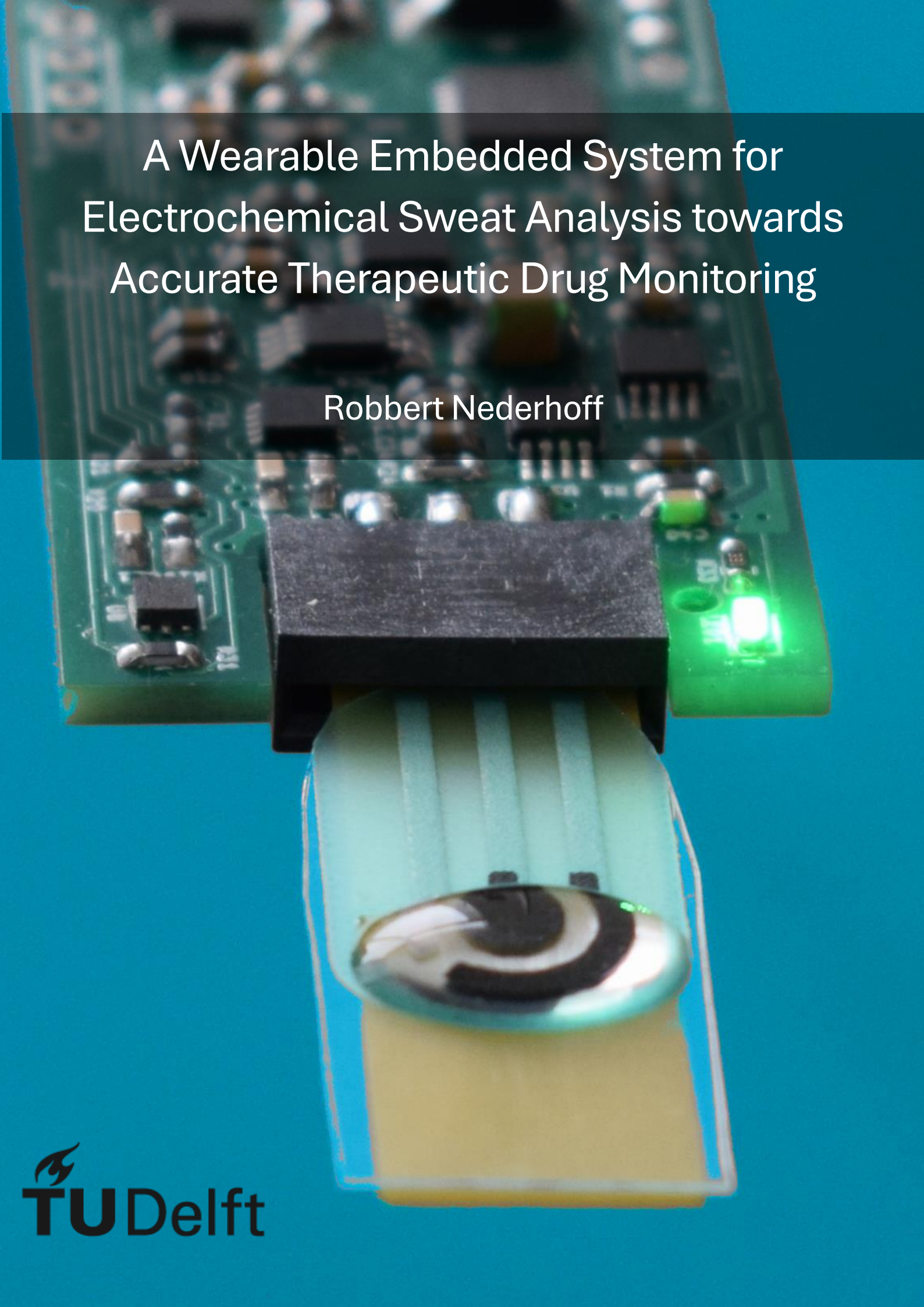

A Wearable Embedded System for Electrochemical Sweat Analysis towards Accurate Therapeutic Drug Monitoring

Robbert Nederhoff

TU Delft

A Wearable Embedded System for Electrochemical Sweat Analysis towards Accurate Therapeutic Drug Monitoring

Robbert Nederhoff

A thesis presented for the degree of
Master Embedded Systems

Student number:	5409845	
Project duration:	12 February 2024 – 16 October 2024	
Research group:	Electronic Instrumentation	
Thesis committee:	Dr. ir. A. Bossche,	TU Delft, supervisor
	Prof. P. J. French,	TU Delft
	Dr. ir. A. S. M. Steijlen,	TU Delft
	Ing. J. Bastemeijer,	TU Delft

Cover: Wearable Embedded System performing electrochemical analysis.

Acknowledgement

I want to express my sincere gratitude to Andre Bossche, Jeroen Bastemeijer, and Annemarijn Steijlen for all their valuable advice, the project, and the overall insightful time I had doing this thesis. I am also deeply thankful to Paddy French and Marc Parrilla Pons for helping me with this project. A special thanks goes to Rens Ursem for being a remarkable colleague during this journey.

Robbert Nederhoff
Delft, October 2024

Summary

The development of wearable systems for non-invasive, real-time therapeutic drug monitoring (TDM) has gained attention due to the limitations of traditional blood-based methods, which are highly invasive for patients. This thesis presents the electronics and software development for a wearable system that can be non-invasive and continuously analyse sweat using an electrochemical technique. The use case comprises monitoring the antineoplastic drug methotrexate (MTX) by creating two intelligent algorithms that can be executed on wearable devices for more accurate measurements. The algorithms were developed to compensate for influences from changes in sweat's pH levels and extract the related MTX peak from amino acids that overlap the MTX signal.

The wearable embedded system that is realised can measure MTX using square wave voltammetry (SWV) and execute the two algorithms. The algorithms are validated with sweat samples and demonstrate the potential for continuous and reliable TDM through sweat analysis. This innovation is a promising leap to non-invasive therapeutic monitoring using intelligent algorithms.

Contents

List of Figures

List of Tables

Chapter 1

Introduction

Therapeutic drug monitoring (TDM) is essential for drugs with a narrow therapeutic drug window. Precise monitoring helps prevent insufficient dosage, which makes the desired treatment ineffective, and high concentrations of drugs can lead to toxicity. The conventional method of TDM involves monitoring the patient, drawing blood at a specific interval, and analysing it in laboratories [1]. While this method has been the gold standard for many years, it is relatively invasive on the patient, time-consuming, and requires vast clinical infrastructure. These limitations show the need for alternative strategies for patients undergoing TDM [2].

As a result, there has been growing interest in continuous non-invasive monitoring that benefits the patient in comfort and optimises the overall drug dosage through real-time monitoring. Wearable technologies can offer real-time feedback, resulting in a more personalised dosage. Sweat is a promising option for use in wearable technologies and TDM. It is an easily accessible biological fluid that can be utilised for continuous drug monitoring. However, sweat contains a variety of components and even drugs. The concentration of certain drugs admitted to patients can be found in sweat and related to their concentration in blood. This offers a more patient-friendly approach to TDM.

Nevertheless, sweat is a complex liquid, and its matrix can make accurately determining the concentration of a specific drug challenging. Despite these challenges, electrochemical techniques are promising for analysing sweat. They are efficiently executed on wearable systems, require no significant amount of power, and can be constructed in such a way that they have a relatively small footprint [3]. Further, the use case in this thesis is the drug methotrexate (MTX), which is used for chemotherapy and autoimmune diseases.

This thesis aims to develop the electronics and software for a wearable embedded system that can perform analysis and overcome some of the sweat matrix's challenging elements, such as changing sweat pH levels and interfering substances. Therefore, novel methods for overcoming these effects should be developed using intelligent algorithms that can be executed on wearables.

The thesis consists of five chapters. After this chapter, the second chapter discusses the fundamentals of voltammetry, the many available voltammetry techniques, and how sweat influences the measurements. Although the chapter contains further information about electrodes and the influence sweat has on them, along with eventually proposed solutions, it is beyond the scope of the thesis. In the third chapter, a prototype is developed, and the complete engineering process is documented. The prototype is for testing and exploration. It is

further used as an example and an important learning step for developing the final wearable. In the fourth chapter, before the conclusion, two algorithms are developed, one for compensating changes in voltammetry measurements due to the change in pH in sweat and a second for extracting the MTX-related peak from interfering substances found in sweat that overleap the MTX signal. This chapter will be published in a journal; it contains an introduction and conclusion with supplements. The last chapter is the conclusion.

Chapter 2

Voltammetry

Electrochemical sensors are the most promising choice for wearable sweat sensors because of their performance cost, miniaturization and broad applicability. Voltammetry is an electrochemical method suitable for detecting electroactive drugs [3]. This chapter deeply explores voltammetry, such as the different types and working principles, and the influences of sweat, a complicated biological fluid with numerous compounds, making it complex for electrochemical analysis [4]. This section additionally discusses electrodes used to perform voltammetry. While this chapter provides essential background information, some details extend beyond the scope of this thesis.

2.1 Fundamentals

The chemical changes in electrochemistry are related to the flow of electrons. These chemical changes are often an analyte's oxidation or reduction (Redox) reaction [5]. In an electrochemical reduction, the analyte is reduced by increasing the energy on an electrode, typically made from platinum, gold, mercury, or glassy carbon, until electron transfer becomes favourable. For electrochemical oxidation, the process is reversed, and electrons are released. The force driving this reaction is the energy difference between the electrode and the agent. The thermodynamic and kinetic parameters can be measured by controlling this force, which is in this case the potential.

$$E = E^0 + \frac{RT}{nF} ln \left(\frac{Ox}{Red} \right) \tag{2.1}$$

In the Nernst equation (equation 2.1), the potential E is equal to the standard potential E^0 of the substance and the oxidised (Ox) and reduced (Red) are from the Redox activity of the system at equilibrium. Moreover, the F is the Faraday's constant ($F = 96485.33212\,\mathrm{C/mol}$), R is the universal gas constant ($R = 8.314462618\,\mathrm{J/mol\,K}$), T is the temperature, and n is the number of electrons. When the potential is changed, the concentration of the analyte is going to a new equilibrium according to the formula. The flow of electrons at the electrodes and the potential at the electrode can be converted into a voltammogram by plotting the potential against the measured current. In figure 2.1, an example is shown of a cyclic voltammogram (CV) where the potential is linearly increased and then decreased, resulting in a voltammogram with an oxidation and reduction peak.

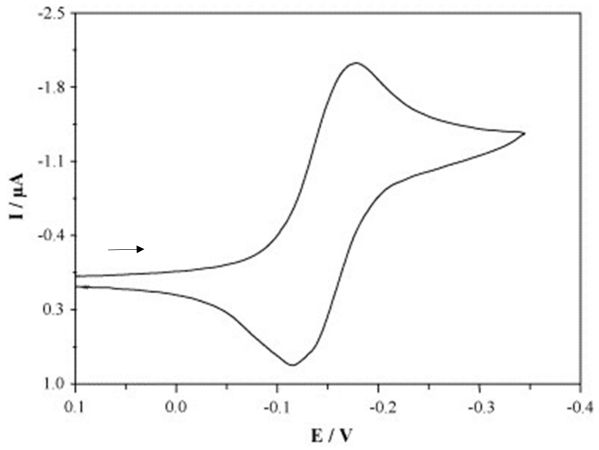

Figure 2.1: Cyclic voltammogram (CV) of riboflavin, which undergoes a reversible single electron transfer [6]. The arrow shows the sweep direction.

In the voltammogram, the potential sweep and current at the electrode show the depletion of the analyte at the electrode. Due to the electrode's diffusion layer, which grows during a sweep, the electron transfer is slowing down. Peaks in current in the voltammogram result from these two behaviours that can be observed during a voltage sweep.

Voltammograms may vary due to factors such as reversibility and the number of transferred electrons and scene rate. When processes are electrochemically reversible, the Nernstian equilibrium is established immediately after applying a potential. Nevertheless, if the reaction is irreversible, it is more sluggish, and more potential is required to observe a reaction. Aside from reversibility, other processes can lead to more intricate voltammograms, such as multi-electron processes and irreversible, coupled chemical reactions, which occur when a chemical reaction takes place immediately after the electron transfer. However, this depends on the analyte being analyzed. Another critical parameter is the scan rate, which leads to higher currents due to the decrease in the size of the diffusion layer. The Radles-Sevick equation defines the relation between the peak current and the scan rate (Equation 2.2).

$$ip = 0.446nFAC\left(\frac{nFvD}{RT}\right)^{0.5} \tag{2.2}$$

The ip is the peak current in ampere, the v is the scan rate (in V/s), the n is the number of electrodes, the A is the surface of the electrode (in cm^2), the D is the diffusion coefficient (in cm^2/s) of the oxidised analyte, C is the bulk concentration of the analyte (in mol/cm^3), F is the Faraday's constant ($F = 96485.33212\,\mathrm{C/mol}$) and R is the universal gas constant ($R = 8.314462618\,\mathrm{J/mol\ K}$) [7].

Different types of voltammetry exist to detect distinct drugs in body fluids with various electrodes. According to Tai et al. [8] and Raymundo-Pereira et al. [4], differential pulse voltammetry (DPV) is commonly employed to detect drugs in sweat. Other methods, such as CV [3], are also suitable for detecting drugs in sweat. Square wave voltammetry (SWV) is another promising technique used in various body fluids for detecting drugs [9] [10] [2].

The voltammetry techniques work by applying various potentials to the electrodes. CV

sets a linearly increasing voltage on the electrodes, reducing the substance. The current continuously increases until the electron transfer slows down due to the diffusion layer. Then, the voltage decreases again linearly, and the current shows the peak of the substance's oxidation. DPV increase the amplitude according to a linear ramp that incorporates steps. Each following step is higher than the previous one (Figure 2.2). The current is sampled before the pulse is applied and similarly after the pulse [11]. The difference between the currents is hereafter calculated. Due to the subtraction, the background current, also named capacitive, charging, or non-Faradaic current, is equally subtracted. This procedure is distinguishable from cyclic voltammetry, where the non-Faradaic current is always present in the background and which is influenced by the scan rate [7] [12]. A significant advantage of DPV is low capacitive current, resulting in higher sensitivity. The small step sizes in DPV are favourable for discriminating analysts that have similar peaks near the same potential due to the narrower voltammetric peaks it has [5].

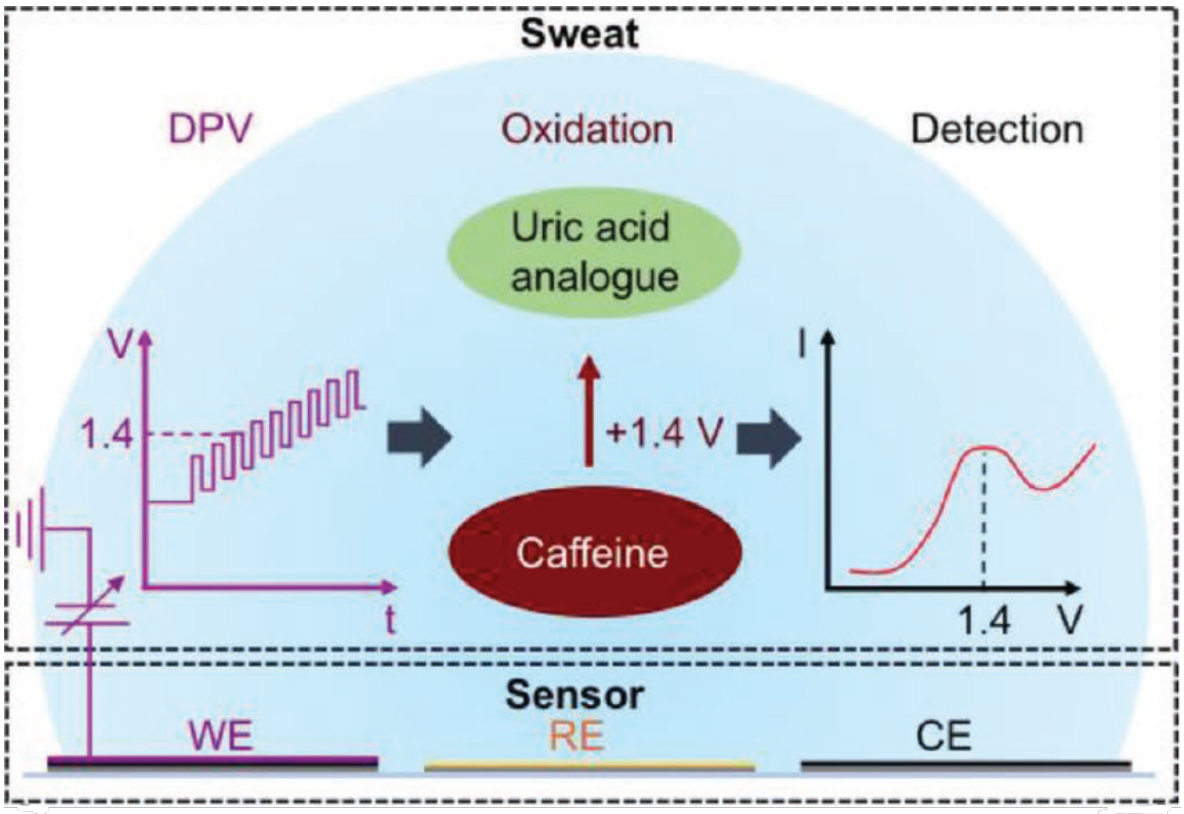

Figure 2.2: A wearable sweat sensor detects caffeine using differential pulse voltammetry: purple for the applied potential and red for the signal measured. The peak of the reaction is around 1.4 V [8].

Square wave voltammetry (SWV) is, according to Simões and Xavier [12], one of the most sensitive pulse voltammetry techniques. SWV is considered a particular type of DPV. It is a large-amplitude differential technique with a combined square wave and staircase potential applied to a working electrode. In Figure 2.3 a, the potential that is applied is shown, where E_{sw} is the amplitude of the square wave, E_{sc} is the step of the staircase, and I_1 and I_2 are the current measurement moments. In b, the desired signal is obtained by subtracting I_1 and I_2, which are measured. SWV can obtain high sensitivity due to the minimal contribution of non-faradaic currents. The low faradic current and the significant time between the current sampling make this technique more sensitive than other electroanalytical techniques. Therefore, SWV is employed as an electrochemical measurement technique in diverse research disciplines [13].

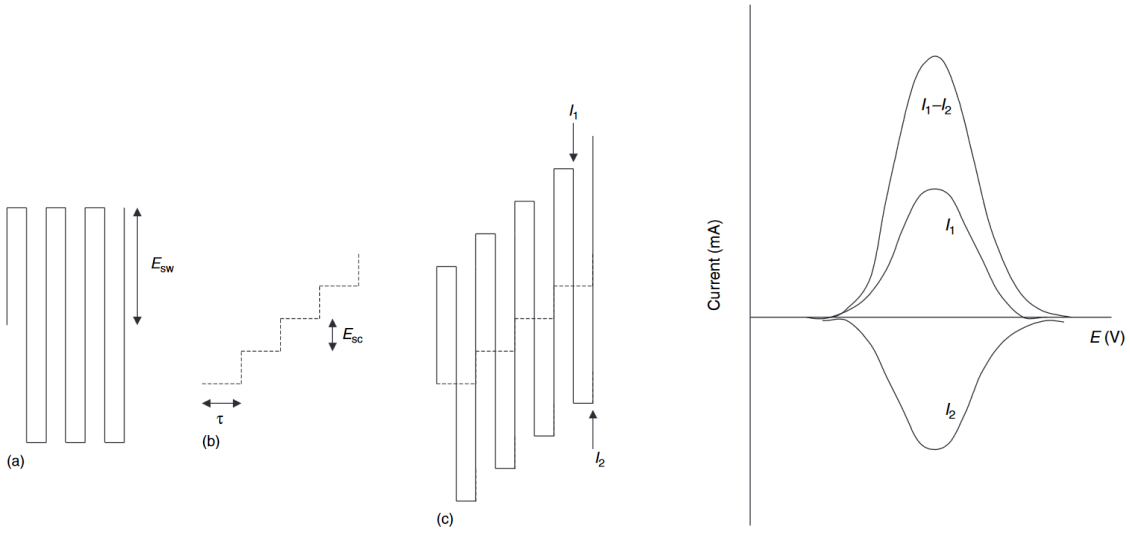

a **b**

Figure 2.3: **a** Applied potential in square wave voltammetry (SWV) with (a) the waveform, (b) the staircase, and (c) the combined waveforms that result in the used potential. **b** The signal that is measured in square wave voltammetry [14].

2.2 Influences of Sweat

Sweat is a complex biological fluid for electrochemical analysis because it contains many substances, including proteins and salts, which can react with the electrode, leading to biofouling that may inhibit electron transfer and decrease electroanalytical performance [4]. Additionally, the measurement of the analytes can be altered in sweat by factors including pH and temperature [3] [15] [11] [16]. Sweat fluctuates in pH between very acidic 2.1 and alkaline pH 8.2 [17], affecting the voltammetric response [4].

2.2.1 pH

pH significantly influences the electrochemical analysis of analytes. This is demonstrated by Raymundo-Pereira et al. [4], where pH variations not only affect the peak current but also shift the peak potential to more positive values as pH decreases, as observed with compounds like uric acid and drugs such as paracetamol and ethinylestradiol (Figure 2.4). This pH sensitivity introduces challenges when monitoring drugs, especially those with narrow therapeutic windows.

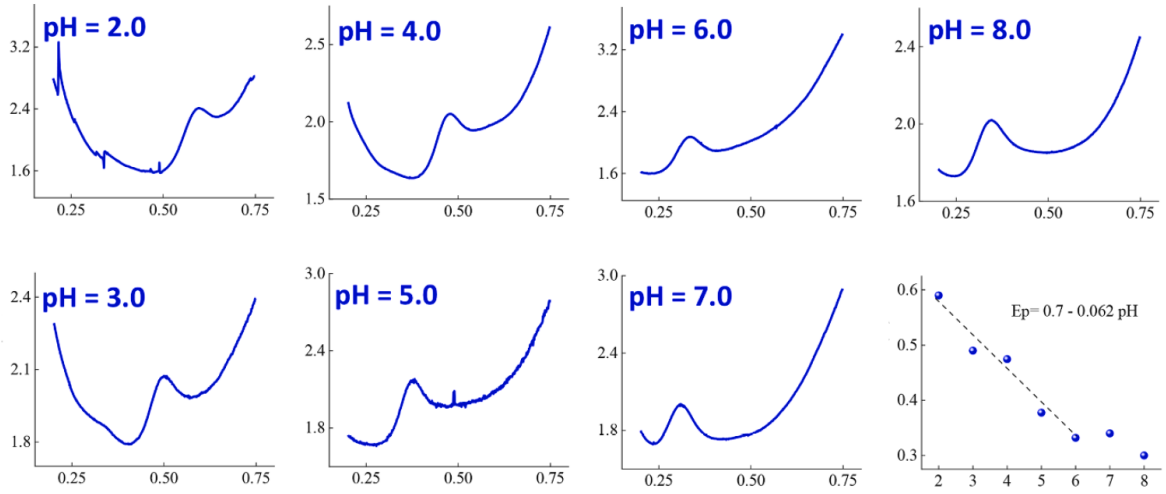

Figure 2.4: The voltammetric response of $5.0 \cdot 10^{-6}$ mol L^{-1} ethinylestradiol at different pH levels [4]. A nearly linear relation is observed between the peak potential and the pH (bottom right).

One promising approach to overcoming pH-related challenges was proposed by Tajik et al. [9], where a buffer solution with a constant pH was used to ensure a stable and optimal voltammetric response. Another innovative method was developed by Yeung et al. [11], who developed a stretchable patch fabricated with electrodes that detect glucose and measure pH and skin temperature levels. Their system corrects any potential errors in glucose measurements in sweat using a pH sensor and the documented relative change of the current for each pH level (Figure 2.5). The glucose concentration can be estimated by compensating the change in current for each pH level [18].

Detecting drug molecules, however, is a significant challenge due to their typically low concentrations in sweat. Despite this, considerable progress has been made in wearable drug-

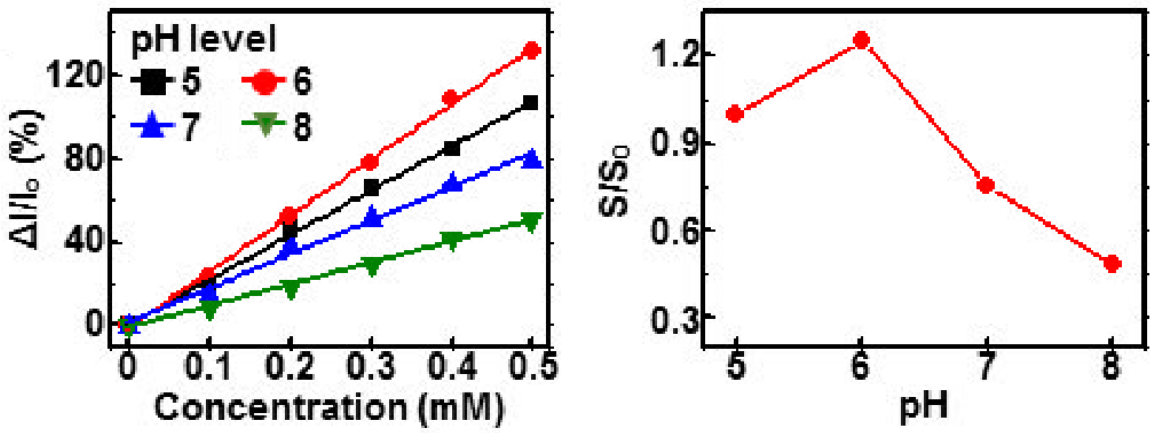

Figure 2.5: Influences of pH on the glucose sensor. Left: The change in peak current (I) of a CV compared to the initial current in percentages of the glucose sensor at different pH. Right: The sensitivity (S) refers to a change in the current of the glucose sensor as a reaction to the change in pH level. The initial potential of the sensor is -0.05 V [18].

sensing systems. For example, one study enhanced electrodes for cyclic voltammetry to successfully detect levodopa, a drug used in Parkinson's disease treatment [19]. A study used a similar method that utilized differential pulse voltammetry to monitor methylxanthine drugs in real-time in sweat [8].

Nevertheless, the detection of drug concentrations in sweat remains complex. The low analyte concentrations and pH fluctuations make stable detection challenging for electrochemical sensors. Despite these difficulties, there is a growing need for susceptible wearable sensors that can monitor low concentrations of analytes in sweat with effective and adaptive sensing mechanisms [3].

2.2.2 Temperature

Temperature influences in voltammetry are even described in its fundamental parts, such as the Nernst equation, where the temperature change has a linear relation with the potential of the electrochemical cell. Another fundamental formula which uses temperature is formula 2.2, which is regarding the peak current. Nevertheless, the temperature and peak current relationship in this formula is not linear [7]. Nonetheless, the temperature probably has more influence on the measurement, as it has been shown to influence the concentration of the analytes [3]. Figure 2.6 shows the impact of temperature on various measurement techniques of diverse analytes. In figure 2.6 A, an amperometric sensor measures glucose and lactate [20]. The temperature is compensated, which reduces the effect. Figure 2.6 B shows the effect of temperature by analysing uric acid and tyrosine using DPV [21]. Meanwhile, Figure 2.6 C illustrates the relationship between the peak current and the temperature for measuring heavy metals in body fluids [22]. The method used is stripping voltammetry, similar to voltammetry, though the electrode selectively reacts with the analyte [23]. Lastly, Figure 2.6 D uses CV [18], and the relationship between different temperatures shows a nearly linear behaviour (a gradient shift) between the glucose concentration measured in sweat and the relative current.

The temperature influence in all these figures shows nearly linear responses. Where the

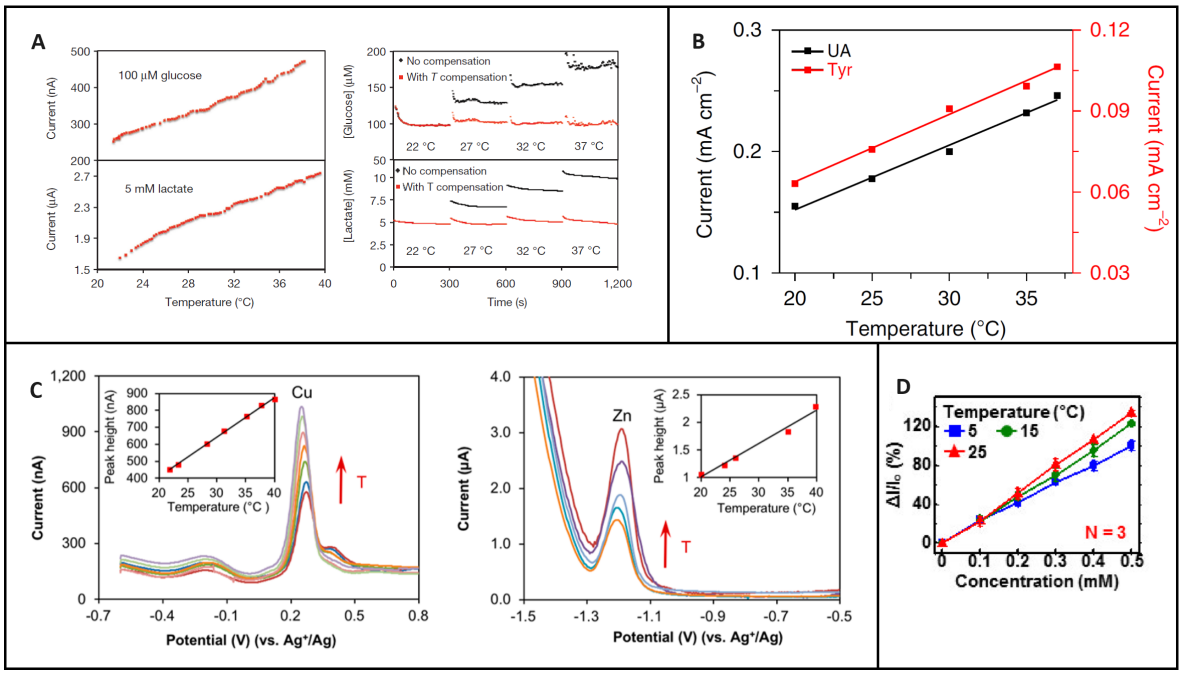

Figure 2.6: Temperature influences on electrochemical measurement techniques.

increase in temperature results in a rise in the signal. Therefore, temperature compensation is essential for reliable data [22].

2.2.3 Biomarkers

Sweat contains several biomarkers such as electrolytes, metabolites, drugs, trace metals and other analytes such as hormones and proteins. Sweat consists of nearly 99% of water molecules, making it the most common component. The most abundant electrolytes in human sweat are Na^+ and Cl^-. Na^+ is a marker for the imbalance of electrolytes in the body and regulates several things, such as pH. Metabolites in sweat, such as glucose, can be used to measure the sweat rate. Further, some drugs resemble toxins that the body excretes and, in certain instances, can be detected. Metals in sweat can reflect diet, heat stress and physical exercise. Proteins and hormones, such as cortisol, neuropeptides, and cytokines, are also present in sweat [3].

Besides that, sweat constituents interrupt drug detection because the individual Redox potential of these molecules may interfere with detecting specific drugs. For every type of drug, an interference study should be performed (Figure 2.7). For example, in Tai et al. [8], methylxanthine was measured in the presence of urea, glucose, lactic acid, ascorbic acid, and pilocarpine (commonly used to induce sweating). The results show these biomarkers do not influence the peak current during detection.

Electrolytes in the solution are crucial not only for maintaining the body's physiological functions but also for enhancing the conductivity of the electrochemical system. Electron transfer occurs at the electrode, migrating the electrolyte to balance the charge and complete the electrical circuit. Therefore, it is essential to have a high concentration of electrolytes; without them, the solution will be resistant to charge transfer and increase the ohmic drop.

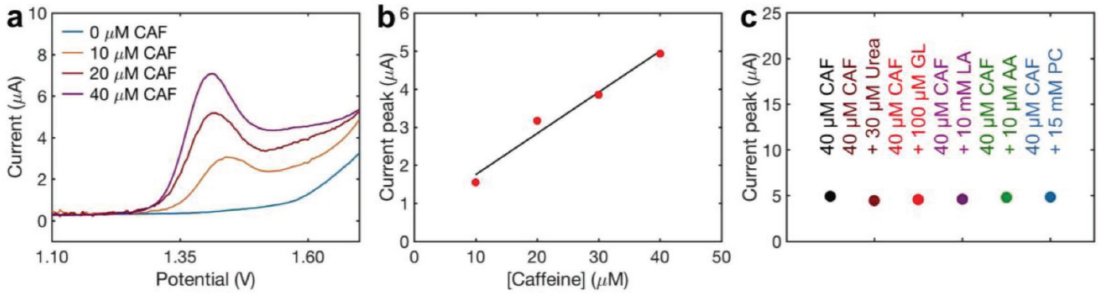

Figure 2.7: a: shows the DPV of methylxanthine at different concentrations. b: shows the linear relation between the peak current and the concentration. c: shows the interference study of methylxanthine [8].

This can influence the measurement accuracy due to the resistance between the working and reference electrodes. Another influence that can change the accuracy is the movement of the analyte, which is not beneficial because it makes the electrochemical process irreversible. Mass transport is the movement of the analyte. This should be less than the electron transfer to make the reaction not irreversible. Furthermore, this movement of the analyte is due to three factors: convection, migration, and diffusion. These are mainly minimised by reducing stirring or vibration and using high enough electrolytes in the sample [7].

Nevertheless, biomarkers can interfere with the responses, whereas an interference study can map these biomarkers that interfere. Further, changes in temperature, pH and electrolyte concentration can interfere with the measurements. However, temperature has a nearly linear relation, whereas biomarkers and changes in pH probably do not, which poses a more complex challenge to overcome.

2.3 Electrodes

The three-electrode setup of a chemical cell consists of a working electrode where the analyte reacts, a reference electrode, which is the point where the potential of the other electrodes can be measured, and a counter electrode used as a collector for the reaction (Figure 2.8) [3]. This section discusses the electrodes' composition, biofouling and the (electrical) cleaning method for repeatability.

Screen-printed electrode-based sensors are affordable and portable and can accurately determine various analytes. The sensitivity is confined by the different technologies used for distinct target analytes. For drugs, mostly carbon-based electrodes are utilised [24]. Reference electrodes usually combine silver (Ag) and silver chloride ($AgCl$), which is stable and affordable. However, factors such as reproducibility, contamination on the surface, and manufacturing limit the electrode quality [25]. Yet, due to the low cost, disposability is advantageous [26]. Despite this, doing several measurements for TDM without constantly replacing the electrodes can be favourable.

A potential threat of performing several measurements is the increase of biofouling. Voltammetric responses of the redox signal can be buried or distorted by electroactive agents in biofluids, a process called biofouling. It arises from the adsorption of these agents from

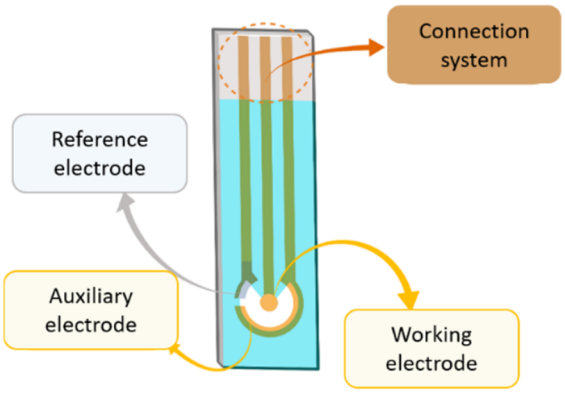

Figure 2.8: Screen-printed electrode with working, reference and auxiliary (counter) electrode and the Connection system for attaching the electrode to the potentiostat [25].

different biomarkers, such as proteins, onto the electrode surface. When creating the surface of the sensing interface with particular types of components, parameters such as background current, biofouling, potential window, and operational stability can be altered. Due to this, the repeatability of the sensors can be extended, and this is accomplished in Lin et al. [27], where by using electrodes with hydrogen-terminated boron-doped diamond (H-BDDE) and a Nafion coating, the distorted signals were surpassed. The repeatability after eight trials had a standard deviation of a mere 4%.

The repeatability of the electrodes can be enhanced by cleaning the electrodes periodically. In Stan et al. [25], the electrodes are cleaned with acetone, ethanol, and hydrogen peroxide or by electrochemical methods. Other methods have also been tried. However, some treatments can lead to low sensor repeatability and affect the insulating layer of the electrode. For solvents, the cleaning of the electrode consists of depositing twice the cleaning product on the electrode and leaving it to work for a specific time. A buffer solution is used to rinse off the solvents. The electrochemical cleaning method by applying negative sweeps is very efficient in removing contamination as well. It improves the senors effectiveness by improving the electrodes' surface and enhancing the target analyte's detection limit. However, increasing the cycles may deteriorate the electrodes. Overall, electrochemical cleaning of the electrodes appears to be a practical method that can be applied.

In conclusion, this section shows that screen-printed carbon and silver/silver chloride electrodes are commonly used for drug detection. Biofouling can cover the electrodes, distorting the signal. Removing contamination by applying negative sweeps is a cleaning method that can be utilised without additional procedures.

Chapter 3

Measuring System

This chapter first delves into existing voltammetry systems, including measuring systems and their setup. Hereafter, two systems will be developed for this project. The first one is the prototype: a multichannel experimental voltammetric measurement system. This system will be explained extensively. The other is a wearable that can execute voltammetric measurements and output the molar concentration of MTX, which is based on the prototype.

3.1 Existing Voltammetry Measuring Systems

Wearable devices are composed of electronics and software that control electrochemical cells and retrieve data and are the essential part of a wearable device [3].

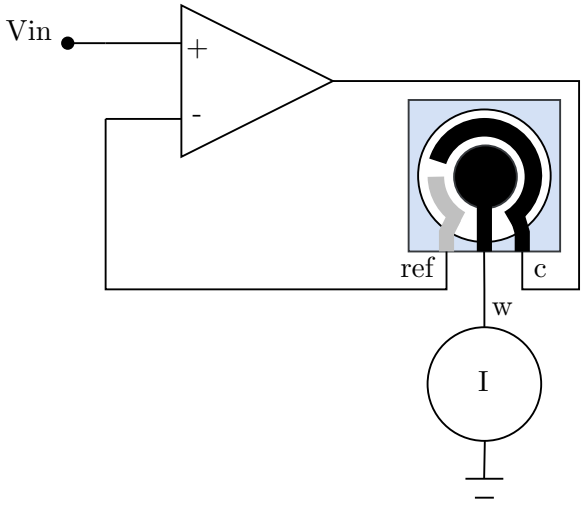

Figure 3.1: Working principle of the electronics used in an electrochemical cell with reference (ref), counter (c) and working (w) electrode.

Electrochemical electronics' working principle consists of an amplifier and a current meter (Figure 3.1). The current meter (working electrode) connects the electrode to the ground, and the amplifier applies a potential to the electrode (counter electrode). The amplifier uses the reference electrode to control the potential according to the applied input potential. The current meter can measure the current related to the Redox reaction across the counter and

the working electrode. In existing systems, the current meter is a trans-impedance amplifier (TIA) that works as a virtual ground, filters the signal, measures the current and outputs it in a voltage. The TIA is connected to a microcontroller through an analog-to-digital converter (ADC), which can process the voltage that is related to the current [20] [28] [29]. The feedback system is primarily utilised for the potentiostat, which is controlled by an input voltage. However, slightly different circuits can be used. In Snizhko et al. [30], inverting and non-inverting amplifiers are discussed. The inverting amplifier (Figure 3.2 A) has the non-inverting input of the control amplifier (CA) connected to the ground, and the feedback is linked via a resistor to the same input as the input voltage is applied. The operational amplifier (opamp) input voltage and feedback are attached to different opamp inputs for the non-inverting amplifier (Figure 3.2 B). The inverting amplifier is preferred in this case over the non-inverting amplifier, due to its lower common-mode rejection ratio (CMRR) error. However, a voltage follower is needed to buffer the reference electrode voltage, which requires additional components and increased power. In practice, the measurement frequencies of wearable sensors are relatively low (around 20 Hz [21]), which reduces the impact of CMRR error at these lower frequencies [31]. Further, numerous wearable systems utilise non-inverting amplifiers [4] [21] [8] (Figure 3.2 B).

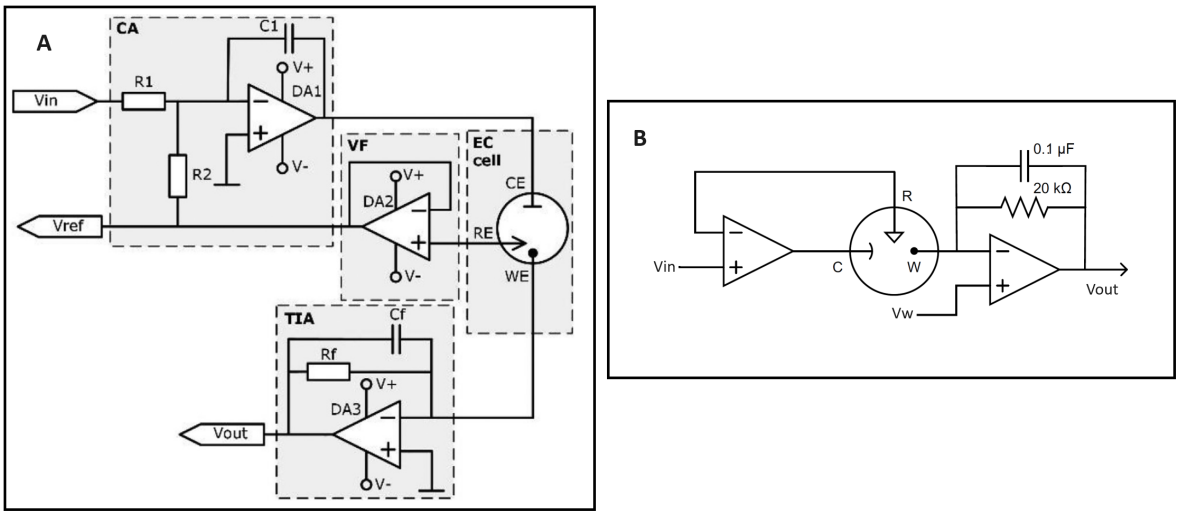

Figure 3.2: Circuit diagrams of the sensing electronics where Vin is the control voltage, Vw is the working electrode potential, and Vout is the voltage read by the ADC. In A. An inverting amplifier as a control amplifier with a voltage follower as feedback and a TIA for current registration [30]. B. Non-inverting feedback amplifier as control amplifier and a TIA for measuring the current [21].

Therefore, to realise a sensitive measurement system, a TIA is employed for the current measurement, and an inverting amplifier is employed as a control amplifier. Although the response frequency is around 20 Hz, a non-inverting amplifier is a better consideration for miniaturisation due to fewer components. Filtering to remove noise is vital to a sensitive system. This should all be considered in the design.

3.2 Design and Development of the Prototype

This section presents the objective and requirements of the voltammetric prototype and clarifies the prototype's design and software.

3.2.1 Design Objectives

The objective is to develop a prototype for conducting electrochemical analysis on a small scale with effortless testing capabilities and to utilise this prototype for further scientific exploration. The prototype will include temperature and pH sensors for calibration and characterization. Additionally, the analysis software can be easily modified as needed. The prototype may be considered an initial phase in developing the final embedded wearable device.

The requirements are listed below, and the prototype must meet them to achieve its purpose.

1. The system can sweep a voltage of 3.3 VDC voltage with a changing vertical ground (both negative as positive) on custom-made screen-printed electrodes containing carbon (C2030519P4) working and counter electrodes and silver/silver chloride reference electrodes (C2040308P2) of Sun Chemical, United States.
2. The system must measure the current through the electrode within a range of 10 to 0 μA.
3. The system must have a temperature sensor that can measure between 20 and 40 degrees Celsius.
4. The system should have a circuit to measure pH from 2 to 8 with screen-printed electrodes.
5. The system should support a sampling frequency of at least 200 Hz (10 x 20 Hz).
6. The printed circuit board (PCB) must be powered with 5 VDC, while the opamps must be supplied with a voltage higher than 3.3 VDC to ensure stability.
7. The system design should contain a footprint of an Arduino Nano for the microcontroller.
8. It should support 4 voltammetric sensors.
9. The voltage on all the electrodes should be measurable for research purposes.

3.2.2 Design Consideration

This subsection presents the design considerations for the major hardware components, the potentiostat and the pH sensor.

Potentiostat

The potentiostat is the major element of the prototype. The different designs are stated in section 3.1. The design with a non-inverting feedback amplifier as a control amplifier and a TIA for measuring the current is also used for the prototype. Due to the advantages it represents. In figure 3.3, the Vin and the Vw, which acts as a virtual ground, should be controlled by a digital-to-analog converter (DAC). The Vout outputs the voltage, which is the product of the current and the resistor. Measuring the Vout and the Vref with an ADC provides all the information about the electrode.

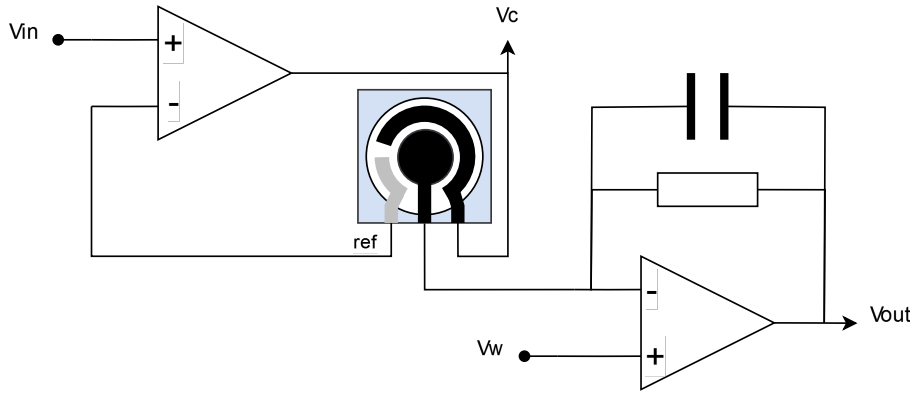

Figure 3.3: The circuit of the potentiostat, with as control amplifier a non-inverting amplifier and for measuring the current a transimpedance amplifier (TIA).

Selecting the potentiostat's components, consisting of a resistor and capacitor, is challenging due to various factors such as frequency (due to the components acting as a filter), potential, and current ranges. The sampling frequency is set at 200 Hz, and the cut-off frequency should be higher than this frequency when selecting the resistor and capacitor. Further, the potential and current ranges should be selected. These are derived from Figure 3.4, which shows a SWV of the use case methotrexate (MTX). The amount of 100 μM in Figure 3.4 is relatively high because, in sweat, only around 5 is found [32]. Nevertheless, this upper limit can be used. The voltage range of the voltammogram and thus of the potentiostat is generally between -0.1 and 1.2 V and the current is assigned to a maximum of 10 μA, which is more than sufficient, as seen in Figure 3.4. However, the forward and backward currents are typically measured. These are slightly higher than the resulting voltammogram created by subtracting the backwards from the forward current.

Applying the voltage to the potentiostat with the DACs can again affect the values of the components. The voltage applied on the circuit is measured from the reference to the working electrode. Further, the TIA adds the voltage applied to the input to the output, which overcomes negative voltages but makes selecting the components and controlling the potentiostat complex. Applying with the DAC a fixed voltage on the TIA and creating waveforms with the control amplifier with the DAC is the most straightforward method, but the signal must be inverted. However, applying a fixed voltage on the control amplifier and controlling the TIA removes some complexity. The best method for positive voltages is setting the control amplifier's input to zero, and the TIA can then sweep the potential. If the resistor has a high value, the voltage on the ADC would be too high. When a negative voltage is required, the control amplifier should apply a higher voltage than the start value of the TIA.

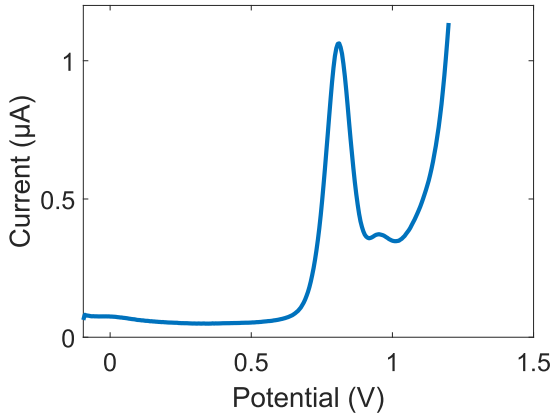

Figure 3.4: Square wave voltammogram of 100 μM MTX in PBS 7.4 pH buffer with 0.1 M KCl.

The voltage on the output is a product of the current from the electrode and the resistor of the TIA. This voltage is added to the voltage applied to the TIA (Equation 3.1, with I the current from the electrode). If the voltage decreases overly far, the voltage will be negative, which is impossible in this circuit.

$$Vout = Vw - I \cdot R \tag{3.1}$$

Therefore, using a 150-kiloohm resistor gives a 10 μA current at 1.2 voltage and output of 3 V. A higher resistor will approach the limit. Nonetheless, the resistor and the voltages applied to the non-inverting amplifier and the TIA can be easily changed to fit the other use cases. For now, 150 kohm and a capacitor of 470 pF are applied. The cutoff frequency is above 2 kHz, higher than those applied to the circuit.

pH sensor

The pH sensor can produce a negative voltage (Figure 3.6). A circuit that can avoid negative voltage, simplifying the total circuit (Figure 3.5). Therefore, a voltage follower (A1) is chosen, which works as a virtual ground and ensures the voltage measured on the other electrode (w) is always positive. The voltage on this electrode is amplified with a non-inverting amplifier (A2) and fed to an ADC (Figure 3.5). The resistor R1 is connected to the output of A1, which prevents the non-inverting amplifier from amplifying the offset (virtual ground).

The resistors in the circuit are selected corresponding to the simulation in figure 3.6. The lowest potential is pH 8, and the highest in the figure is from pH 4. Unfortunately, lower pH levels, such as 3 and 2, are not measured. However, the difference in potential between the pH levels is around 80 mV, meaning that the highest potential at pH 2 will be 160 mV, added to the 230 mV, resulting in 390 mV. The voltage divider's voltage is 4.2 VDC, and the resistors are chosen to be 20 kohm for the top resistor (R4) and 2.7 kohm for the bottom resistor (R3), which produces a virtual ground of 0.5 V. The lowest voltage would be 0.4 V, and the highest would be 0.89 V. The non-inverting amplifier gains 5.4 due to the selected resistors, 7.5 kohm on the left(R1) and 33 kohm at the right (R2) of the inverting input. The output would, therefore, be between 2.6 V and 6 mV, which is in the range of the ADC.

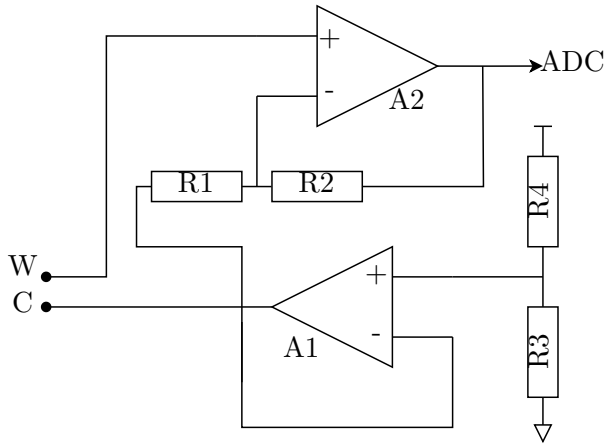

Figure 3.5: The circuit of the pH sensor, with a voltage follower (A1) and a non-inverting amplifier (A2).

Besides, when the voltage of the pH sensor is higher, there is still a margin.

3.2.3 Components and Design

This section outlines the key aspects of the prototype development, focusing on the selection of components, the design of the circuit, and the implementation of the software.

Selection of Components

A detailed explanation of the decisions behind the component selection for the prototype is provided. First, the microcontroller is selected, which controls the entire system and facilitates communication with the PC, is discussed. Next, the chosen opamp in the potentiostats is explained, followed by an overview of the signal converters used to manage the digital and analog signals essential for the potentiostats. Additionally, the temperature sensor and the power supplies responsible for powering the system are chosen.

The microcontroller that is selected for this prototype is an STM32 Nucleo 32 development board. This board has a modest footprint and is compatible with the Arduino Nano. It can be fitted on the prototype, which is advantageous because it does not require further components and keeps the overall prototype reasonably simple. The STM32 is, furthermore, a low-cost, high-performance microcontroller that is effortless to program with the intended software. The selected STM32 Nucleo 32 is the Nucleo-L432KC. This Nucleo 32 has the highest amount of flash memory, which can benefit programming and further software extensions. Besides, the cost of all Nucleo 32 are similar.

Op-amps play a critical role in the prototype design. Key design considerations include the slew rate, offset voltage, input bias current, package, supply voltage, offset drift, input offset current, noise, and price. The most suitable amplifier was determined using the Analog Devices (United States) product selector, with the ADA4500-2 chosen as the op-amp. These op-amps from Analog Devices can be validated in LTSpice and integrated into the design using KiCad, both offering robust support for Analog Devices components.

For the ADC and DAC, the TI part selector (Texas Instruments, United States) was utilised due to Texas Instruments' extensive datasheets that facilitate efficient communication

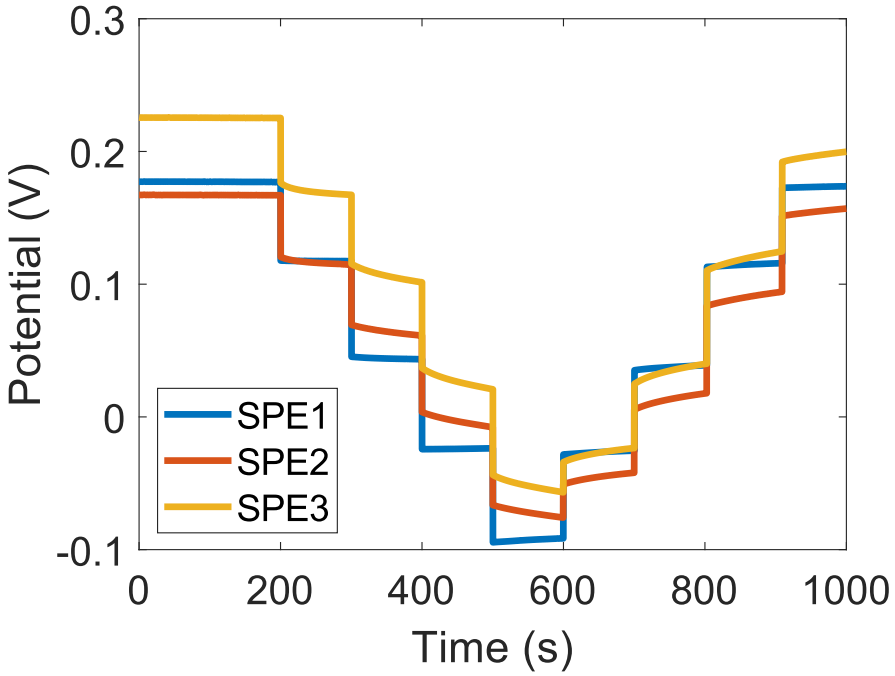

Figure 3.6: The potential measured with 3 electrodes of various levels of pH. pH 4 give the highest and pH 8 the lowest potential.

with the ICs. The selection criteria focused on resolution, sample rate, package, number of channels, reference voltage, supply voltage, and price. Based on these factors, the ADS7066 was selected as the ADC, offering 8 channels, while the DAC80504 was chosen for the DAC, providing 4 channels. Therefore, two DACs were included in the final design.

The temperature sensor is selected using the TI product selector (Texas Instruments, United States), which is preferred because it delivers comprehensive datasheets for communicating with the ICs. The temperature sensor should be reasonably priced and need the highest accuracy. Therefore, the TMP117 was selected as the most accurate product according to the product selector.

The microcontroller board will supply the entire prototype via USB. Thus, 5 VDC powers the microcontroller board and can be utilised as an output power supply for the other prototype components. Furthermore, the microcontroller also has a 3.3 VDC regulator that feeds the microcontroller, which can also be used as an output power supply. However, a higher voltage than 3.3 VDC is needed for the operational amplifiers to provide an adequate margin for powering the electrodes. A regulator further removes additional noise from the USB and provides a higher voltage than the 3.3 VDC. Therefore, the TPS7A20 is chosen because it has, according to the TI product selector tool (Texas Instruments, United States), the lowest noise of all low-dropout regulators (LDO) in the range of 5 VDC input and a higher than 3.3 VDC output. However, the output voltage of the LDO is 4.2 VDC, which is the only one that the supplier has in stock (Mouser Electronics, United States). Additionally, the TPS is utilised to power other components, such as DACs and ADC, evenly distribute the power supply from the TPS and the 3.3 VDC regulator on the microcontroller board. In addition, powering the ADS7066 (Texas Instruments, United States) with 4.2 VDC protects it even for

higher voltages on the inputs than 3.3 VDC, because the the maximum voltage on the input is equal to the supply voltage.

Circuit Design

The hardware design consists of schematic design and printed circuit board (PCB) design. The schematic design comprises component selection, schematic design, and circuit simulation. The circuit and components for the DAC, ADC, power regulator and temperature sensors are designed and selected according to the datasheets. A voltage reference should be employed for more accuracy and precision for the DAC and ADC. For simplicity, a 3.3 VDC voltage reference is selected and used by both the DAC and ADC. The chosen voltage reference is recommended in the ADC datasheet, which is a REF6030. This circuit for the components is additionally created according to its datasheet. Filters on every ADC input are applied according to the datasheets, which are also added to the inputs of the opamps to remove noise. The cut-off frequency is significantly higher than the frequency used for the opamps, and the capacitive load of the DAC is below its limit. Further, LEDs are added to signalling the power supply's operational state. In appendix C A5, the schematics are shown, and in figure A6, the PCB design is shown.

3.2.4 Software Development

The software is a crucial part of the prototype, and this chapter discusses its organisation, design and implementation.

Organisation

An STM32 microcontroller was chosen for the microcontroller, which is supported by an STMicroelectronics integrated development environment (IDE) named STM32CubeIDE (STMicroelectronics, Switzerland). The framework provides peripheral configuration, code generation, code compilation, and debugging features. It is based on the Eclipse/CDT framework, the GCC toolchain for development, and the GDB for debugging. In addition, it allows for the integration of several plugins. Further, a hardware abstraction layer interacts with the upper layer (applications, libraries, and stacks) via a set of application programming interfaces (APIs).

Software design

The prototype's most crucial component is the four potentiostats. They can usually be set to a specific waveform by selecting various parameters, similar to the potentiostats from PalmSens [33], primarily utilised by the University of Antwerp and which inspire the prototype. The waveforms the prototype needs to produce are cyclic, differential pulse and square wave voltammetry. These waveforms are primarily used according to chapter 2.1 for electrochemical analysis of drugs. Moreover, the potentiostats can be employed in two distinct modes, controlling one or more potentiostats separately with different parameters, including waveforms or controlling one or more potentiostats simultaneously.

Besides the prototype's potentiostats, it contains a pH sensor with several adjustable settings. Changing all these parameters and receiving data from the potentiostats, pH sensor, and temperature sensor should be uncomplicated and readable for further data analysis.

Therefore, a command-line interface (CLI) is selected to change all these parameters and get the data in a practical and readable format from the potentiostats, pH sensor, and temperature sensor. Figure 3.7, shows the flow chart for the CLI.

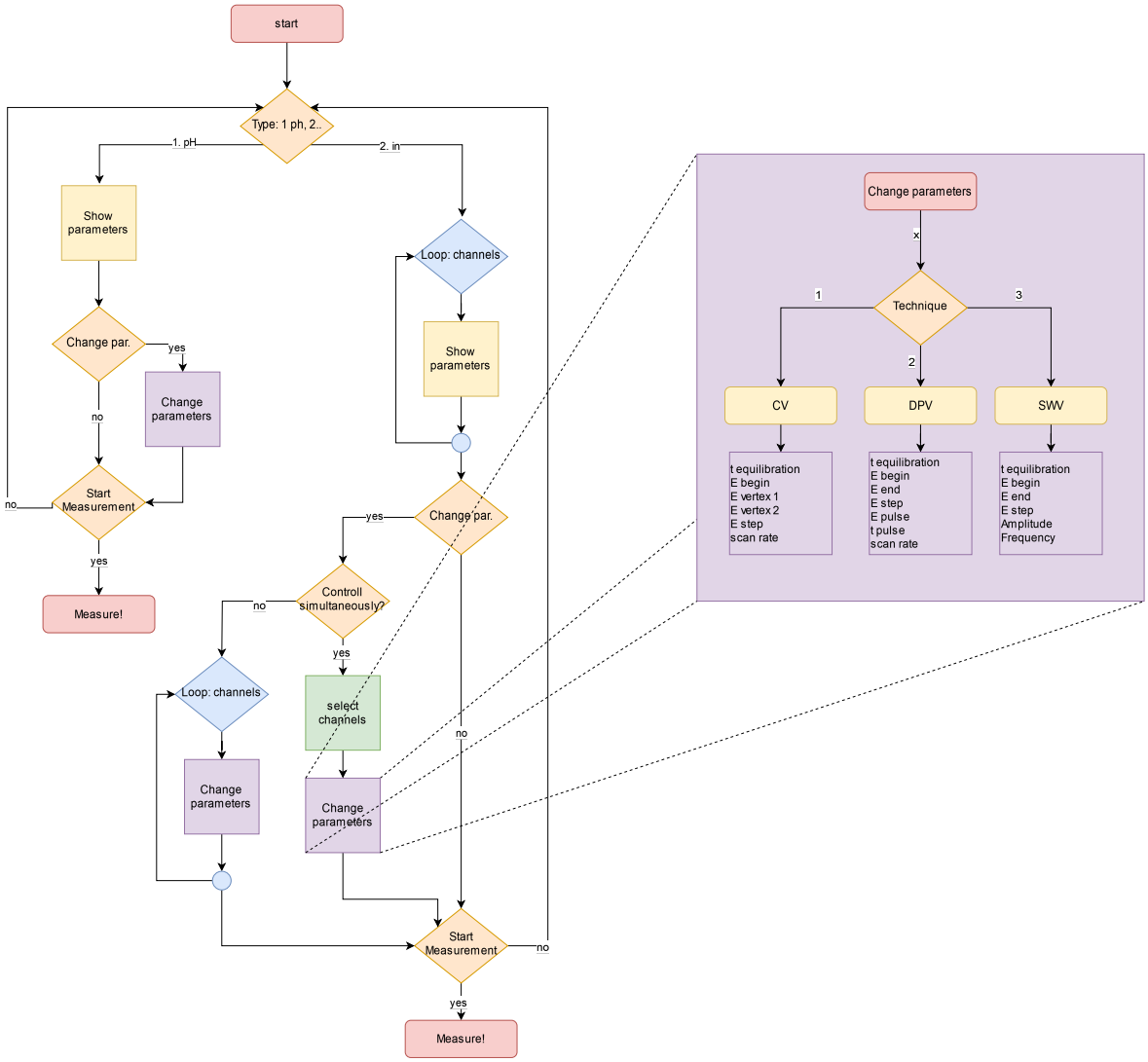

Figure 3.7: The flow chart of the prototype's software.

Since multiple processes are simultaneously executed, the code becomes more complex. For example, the potentiostats' various waveforms must produce and communicate with the PC. Therefore, a real-time operating system (RTOS) is used. FreeRtos is the RTOS already implemented on the STM32 and, hence, utilised for this project.

The produced waveforms need to meet the processor utilisation limit; otherwise, the waveforms cannot be produced. In Figure 3.8, an example is shown of the timing of a square wave voltammogram. Prior to a change in the amplitude of the waveform, the microcontroller measures the current through the electrode, after which it changes the amplitude according to the waveform. The FreeRTOS runs at 1000 Hz, which implies that every 1 ms, a context switch can happen. That means that if, for example, the waveform is executed at 10

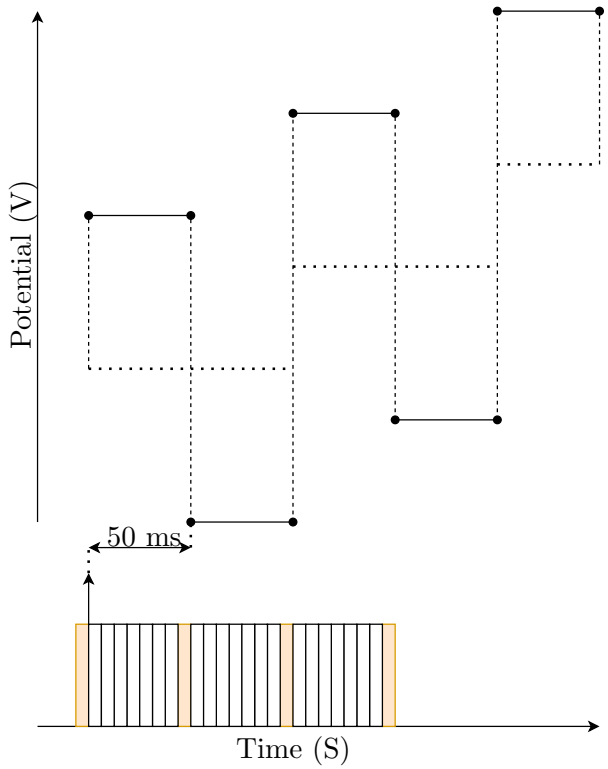

Figure 3.8: Wavevorm of a square wave voltammogram with a timing schema.

Hz, a sequence takes 50 ms wherein the electrode's current is measured and the amplitude of the waveform changes. However, the ADC and DAC take less than 1 ms, which is also the case if the system is set simultaneously, creating the same waveform on several channels. Whereafter, 49 ms remains in every sequence; if the system is set in individual mode, another same-timing waveform can be executed on the other three channels; due to this, the processor utilisation is still below its limit. Although the timing will be similar for differential pulse voltammetry, the waveform's amplitude will be constantly adjusted for cyclic voltammetry. Suppose, for example, the waveform of the cyclic voltammetry has a scan rate of 1 V/s and a step size of 0.01 V. In that case, the microcontroller must change the amplitude of the waveform every 10 ms, which implies that all the channels can run in individual mode cyclic voltammetry without reaching the processor limit. However, if the timing from the various waveforms is increased significantly, the processor utilisation can fall below the limit, and the microcontroller cannot successfully execute the requested waveforms. This is something the user should keep in mind.

The prototype's code consists of various parts, such as the CLI, for controlling the four potentiostat channels that can produce multiple waveforms, the temperature sensor, and the pH sensor. FreeRTOS has several resource management and timing APIs, which are used extensively. The potentiostats, CLI, pH, and temperature sensors run from their individual threads. The program sequence is as follows: the CLI is the first of the threads executed despite its low priority and releases semaphores of all the measuring tasks: the individual potentiostat channels, pH sensor, temperature and the simultaneous potentiostat channel threads. These have higher priority and, therefore, will be executed. However, it will end if

the user did not set up the task. When a task is executed and ends, it releases a semaphore to let the CLI thread know that it is finished; when the CLI thread holds all the semaphores of the tasks, the CLI is executed again. An additional task is the print task that sends the measured data from tasks to the user. This task has a priority between the CLI and the other tasks to make sure that all the data is executed before the CLI is activated and does not interfere with the measuring tasks. These tasks send data to the print tasks by placing the data in a message queue for inter-process communication (IPC), which the print tasks retrieve and send to the serial monitor. Further, the ADC and DAC communicate with the same SPI bus, and therefore, the SPI is operated with a mutex to overcome any race conditions. The code of the entire system is found on GitHub [34].

3.2.5 Realisation and Testing

In this section, the prototype is realised and tested. After receiving the PCB, it is assembled (Figure 3.11), and the software is uploaded to the microcontroller. By setting this in the CLI, the prototype can successfully produce the various waveforms (Figure 3.10). Figure 3.9 shows furthermore the CLI and the exact temperature at the beginning of an SWV experiment.

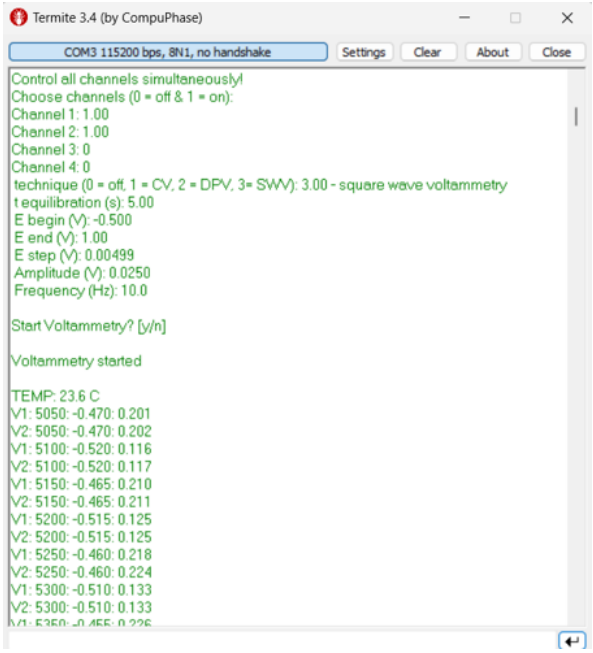

Figure 3.9: The command-line interface (CLI) controls the prototype system for electrochemical sweat analysis, shown in a serial monitor (CompuPhase, The Netherlands). It allows users to configure settings, initiate measurements, and retrieve data from the wearable device.

Further, a test is executed by placing a droplet of 0.8 μl with 0.25 mg/ml APAP on an SPE. The signal starts at -0.5 V and increases in steps of 0.01 V until it reaches 1.3 V. Each step has a square wave with an amplitude of 0.005 V, oscillating at a frequency of 10 Hz. In figure 3.12, the measurement of the prototype is shown. The peak lay, according to [35], around 0.4 V according to the reaction potential of APAP. The peak is lower, probably due to the deprecated solution. Still, the measurement's accuracy and stability are excellent, even though no digital filtering has been conducted. When comparing the measurement to

the voltammograms (Figure 4.1) from commercial potentiostats such as the MultiTrace from PalmSens [36]. The signal-to-noise ratio (SNR) is above 30 dB, obtained with the MATLAB toolbox (MathWorks, United States) by taking a periodogram of the signal and removing the first six harmonics, including the fundamental. This indicates that the signal is 1000 times stronger than the noise, which is significant. However, a 10-kiloohm resistor is applied at the TIA because not MTX but APAP is tested, which provides a higher current. Due to the lower resistor, the ADC does not even utilise its entire bit range. Improvements for the system include redesigning the temperature sensor due to the microcontroller's excess heat influencing temperature measurements and further optimising the code.

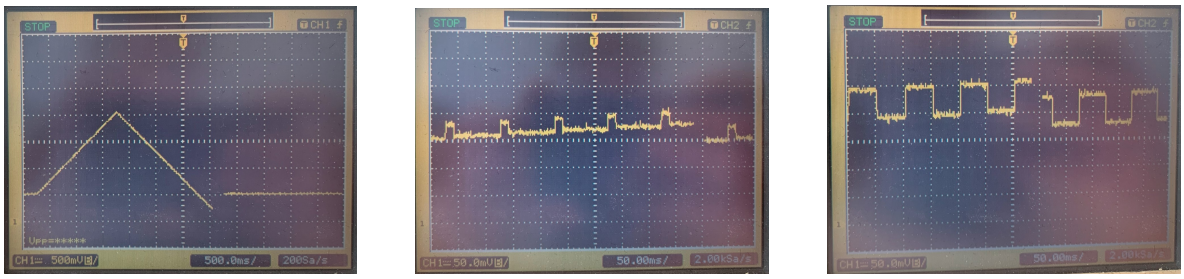

(a) (b) (c)

Figure 3.10: Waveforms generated by the prototype. a) Cyclic voltammogram. b) Differential pulse voltammogram. c) Square wave voltammogram.

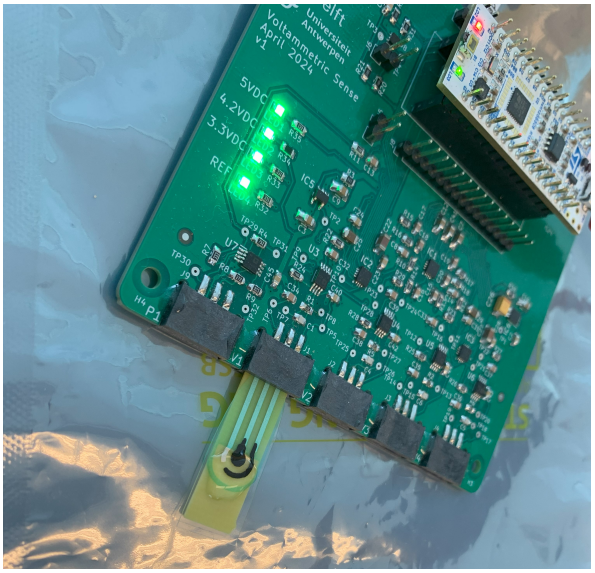

Figure 3.11: Realisation of the prototype running a voltammetry experiment.

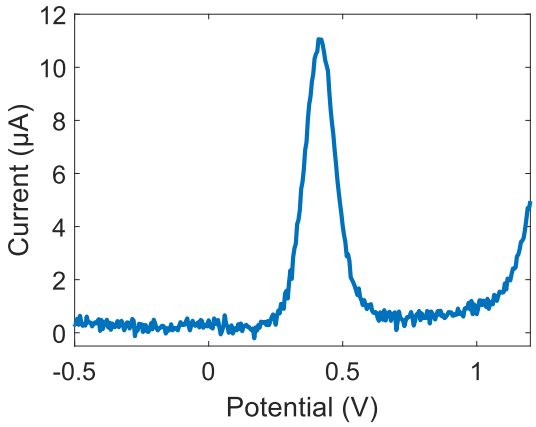

Figure 3.12: Square wave voltammogram of 0.25 mg/ml APAP executed with the prototype.

3.3 Development of the Wearable Device

A wearable device consisting of a single potentiostat was developed as the final measuring system for this project. This wearable incorporates parts from the prototype and is intended to perform electrochemical (square wave voltammetry) sweat analysis and output the exact molar concentration of MTX.

3.3.1 Concept and Design

The device contains similar attributes to the prototype and should be slim and extendable for future research. Therefore, a valid option is to use a USB connection to send and receive data and power the device. However, complex wireless alternatives and powering components are better suited for wearable devices, but they are complex and are not the focus of this research. Therefore, the device should be extendable to include other types of communication and power modules in the future, which is accomplished by reserving a serial data output on the PCB. Further, the wearable design includes, as well as the prototype, a temperature sensor for measuring the ambient temperature, which is helpful for data analysis because the temperature significantly influences the measurement (Section 2.2.2). The design contains an LED for signalling and debugging purposes. The pH sensor circuit is removed from the design because the wearable will only perform voltammetry, and the developed algorithms do not need a pH sensor (Chapter 4). In addition to the design, the conductivity between two electrodes can be measured by shortening the reference and counter electrodes. Thus, the conductivity can be measured between the counter and the working electrode. Measuring conductivity with the prototype was likewise possible due to using an extension board connected to the potentiostat connector. Appendix A explains the motivation for measuring conductivity. For the wearable, precision switches are positioned between the electrode traces to connect the reference to the counter electrode to measure the conductivity. The precision switch IC employed in the design, a TMUX1123, has a dimension of 5 by 3 mm. Therefore, the general size of the design is maintained when this IC is incorporated. Overall, the wearable consists of components similar to those of the prototype. It has a slim, extendable design.

3.3.2 Methods and Design

Selection of Components

The wearable components are similar to the prototype's, including additional changes for the microcontroller, ADC, DAC and power supply. The prototype's microcontroller consists of a Nucleo-32 STM32L432 development board. However, the STM32L432 is still used for wearables as a standalone IC with two program pins for the STM32 Serial Wire Debug (SWD) and the necessary components, such as capacitors. Due to this, the complexity of the design is increased. Nevertheless, the microcontroller's footprint is significantly reduced. The ADC and DAC are changed for ICs with fewer ports to accommodate the one-channel potentiostat. Therefore, the DAC70502 and ADS7946 are chosen and conform to the same criteria stated in section 3.2.3. The wearable includes an additional 3.3 VDC supply because the development board of the prototype comprises such a power supply. For simplicity, the selected power supply is duplicated from the microcontroller development board, which has excellent features (i.e., noise, power, dimensions, and price) compared to the TI product selector tool (Texas Instruments, United States).

Schematics

In appendix D Figure A7 shows the schematic of the wearable. The selected ICs are accompanied by components recommended by their datasheets. Further, the design has a diode for reverse polarity protection and a 4-pin header for serial communication for future expansions.

Figure 3.13 illustrates the layout of the PCB, which measures 50 mm by 25 mm. The potentiostat connector is positioned on the narrower side, making the design suitable for wearing it even on the lower arm. Analog components are placed as close as possible to the connector to minimise interference, while digital and analog traces are separated as much as possible. Additionally, power supplies are placed on the opposite side of the PCB to reduce heat influences. Further, the LED and temperature sensors are on opposite sides of the potentiostat connector gap for optimum use of the minimal design.

Software

The wearable's working principle differs from the prototype's, although functions are reused, such as the SWV functions (Figure 3.14). The purpose of the wearable device is to analyse sweat at regular intervals. As a result, the wearable can be applied in a microfluid setup that continuously measures the MTX concentration in sweat and outputs it. The user can effortlessly adjust the interval and the SWV's settings during the measurements in the CLI. An RTOS is not employed due to the timer and the simplicity of the working principle of this system.

However, the algorithms realised in chapter 4 can only be performed with MTX in sweat. To make the system available for further research, the user can specify if the wearable performs SWV, uses the default voltammogram, or uploads a voltammogram and runs the algorithms with this voltammogram. Further, the time between the measurements can be adjusted. Due to this, the user can use the system not only with MTX but as a SWV wearable for other purposes, showing the vast possibilities of this system. The software can be found on GitHub [34], and the system can be operated with a serial monitor set at 8 bits, 1 stop bit, no parity and a baud rate of 115200.

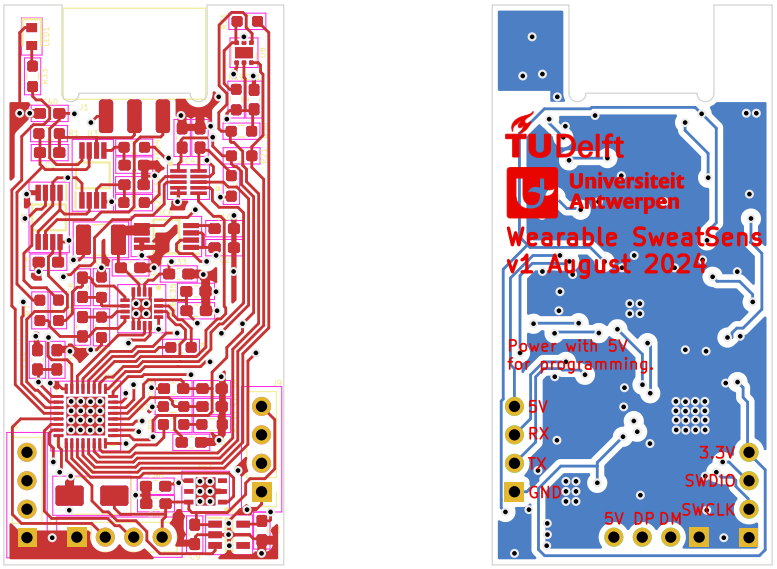

(a) (b)

Figure 3.13: The wearable's printed circuit board (PCB) design. In (a) the top part and in (b) the bottom part of the PCB.

3.3.3 Realisation and Testing

Figure SS9 shows the realised PCB assembled and programmed after receiving it. The system is tested and used in Chapter 4.

3.4 Concluding Insights and Recommendations

This chapter explored the development and implementation of voltammetry-based measuring systems, starting with an overview of existing setups and with the development of two novel systems. The existing setups contained a control and trans-impedance amplifier, and the software for these systems was straightforward. The initial system in this project, a multichannel experimental prototype, proved to be complex but was a foundation for effortless testing and exploration. The second system, a wearable device capable of performing square wave voltammetry, was designed for real-time analysis of methotrexate concentrations in sweat. Nevertheless, improvements are still possible for the prototype and wearable. The code can be optimised for the prototype, and the temperature sensor can be replaced to overcome influences from the excess heat for other components. For the wearable, the abilities to improve on are the following subjects: power management and wireless communication. However, they were not part of the scope of this project. With the development of these systems, this chapter demonstrates how a valuable research platform and a compact wearable device offer means for research and real-time therapeutic drug monitoring.

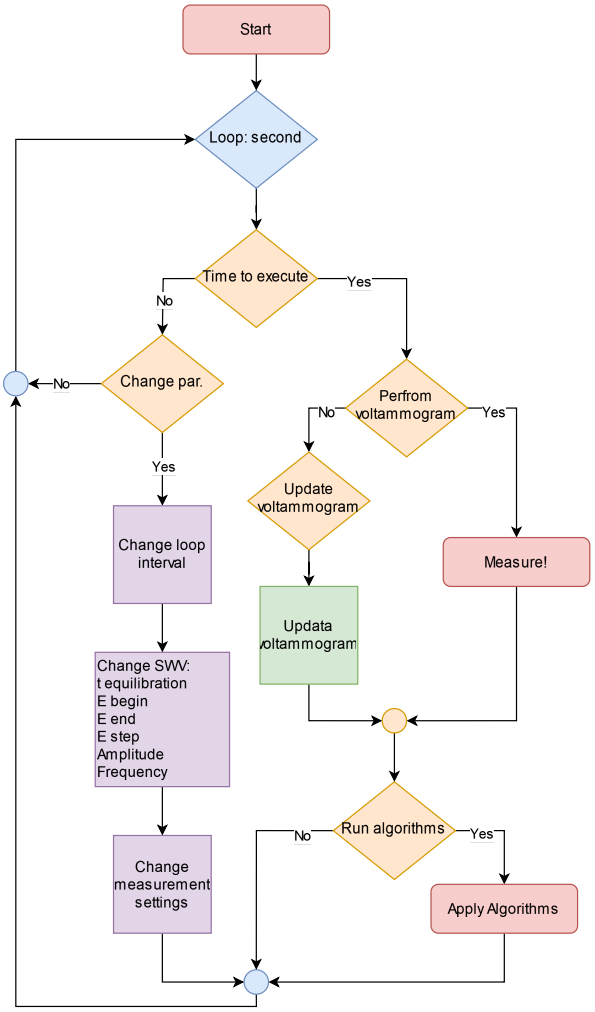

Figure 3.14: Flow diagram of the wearable system's software.

Chapter 4

Data Analysis

This chapter discusses overcoming sweat challenges by analysing them, developing intelligent algorithms to compensate for or overcome them, and applying these algorithms on an embedded system. However, this chapter has the format of a paper because it might be published in a scientific journal. Therefore, it includes its own abstract, introduction, and conclusion, making it an independent chapter. Further, it describes developing two algorithms to compensate for amino acids found in sweat that interfere with the electrochemical measurement of MTX and offset pH changes in sweat. These topics are selected because they are the most challenging problems highlighted in Chapter 2; solving them might be a promising leap in applying wearable systems for TDM.

Abstract

Therapeutic Drug Monitoring (TDM) is a clinical method to closely monitor drugs with narrow therapeutic windows and provide effective therapies while avoiding toxicity. The traditional method consists of drawing blood for analysis, which is uncomfortable and time-consuming, thus challenging for frequent monitoring. Electrochemical sweat sensors are a promising solution as they are non-invasive and can continuously measure drug concentrations. This study explores novel techniques to improve the analytical performance of voltammetric sensors for drug analysis, which can be heavily influenced by the sweat matrix. Changes in pH and interference from amino acids have been shown to impact the measurement. Herein, an algorithm is developed to compensate for potential pH fluctuations in sweat by using the relation between the pH level and the peak potential of the electro-oxidised analyte to estimate the pH and calculate the concentration of the analyte in this study. Methotrexate (MTX) is selected as the model analyte as it is a widely used therapeutic drug in cancer, rheumatoid arthritis, among other disorders. Additionally, peak overlap by distinct amino acids with a similar oxidation potential as MTX is separated by an algorithm that uses Gaussian fitting for subtracting and linear discriminant analysis (LDA) to identify the peak related to the analyte. The results demonstrate that the algorithms are effective for the detection of MTX and present an approach to compensating for sweat matrix-related interferences in wearable sweat sensors, driving development for low-cost continuous therapeutic drug monitoring.

4.1 Introduction

Therapeutic Drug Monitoring (TDM) is a clinical method of optimizing drug dosage to maximize therapeutic effectiveness while minimizing the risk of toxicity. It involves measuring the concentration of specific drugs in biological fluids, traditionally blood or plasma, where the concentration is correlated with the administered dose. TDM is particularly crucial for drugs with narrow therapeutic windows, where even minor fluctuations in drug concentration can lead to insufficient dosing or severe adverse effects [1]. This approach ensures the drug remains within its therapeutic range, considering patient-specific factors such as age, weight, organ function, and metabolic activity [37].

Despite its clinical importance, current TDM methods have significant limitations. They rely on invasive sampling techniques, usually involving blood draws, which can be uncomfortable for patients and impractical for frequent monitoring. Additionally, sample collection, storage, and transportation introduce logistical complexities and costs that interfere with the application of TDM. As the demand for more accessible and frequent monitoring increases, alternative approaches are being explored that provide real-time, non-invasive drug monitoring [2].

Electrochemical sensors have emerged as a promising technique for TDM. These sensors offer several advantages, including simplicity, low cost, portability, and the potential for real-time analysis. Among the various electrochemical techniques are amperometry, potentiometry, and voltammetry. Unlike other methods, voltammetry is well-suited for TDM. It allows for the simultaneous detection of multiple analytes and is suitable for drug detection. Sweat, an easily accessible and non-invasive biofluid, is a convincing choice for TDM. It is produced continuously and can reflect drug concentration changes over time, making it ideal for real-time monitoring through wearable technologies. However, despite its potential, sweat-based TDM faces numerous challenges. One of the primary issues is the relatively low concentration of drugs in sweat, which requires susceptible detection methods to achieve stable and reliable results [3] [11].

A critical factor influencing the performance of sweat-based electrochemical sensors is the presence of interference substances and variations in sweat pH. While sweat is nearly 99% water, its remaining components, such as electrolytes, metabolites, drugs, trace metals, hormones, and proteins, play a crucial role in conductivity and often interfere with accurate measurements [3]. Among these, Na+ and Cl- are the most abundant electrolytes vital for increasing the solution's conductivity and are needed for proper electron transfer at the electrode, where electrolytes balance the charge and complete the circuit [7] [38]. Sweat pH, which can range from 2 to 8 [17], adds another layer of complexity. It significantly influences the electrochemical behaviour of many drugs non-linearly, making it difficult to predict and compensate for these changes [4].

Temperature is another factor that impacts sweat analysis. According to [21], temperature variations tend to be relatively linear and can be compensated for by directly measuring temperature. However, it adds another complexity factor for developing a wearable that can be applied to the entire sweat matrix.

To overcome these challenges, several strategies have been developed. A common approach to remove interference substances is to modify the electrode surface by adding functional coatings or altering the material composition to improve selectivity and sensitivity. These modifications can help shift the sensor's detection window away from regions where interference substances are most active [27]. Another strategy employed for the pH variation

in sweat involves buffering the solution to stabilize the pH before electrochemical analysis [9]. While these approaches have shown promising results, they are complex and probably increase the cost of a wearable device.

Approaches such as machine learning can be optimal. Techniques that have been implemented for electrochemical sensing range from straightforward linear regression to more complex models like neural networks [39] [40]. However, more concise techniques such as principal component analysis (PCA) [41] [42] [43] [44] [45], partial least squares regression (PLSR) [46] [47] [48], support vector machines (SVM) [49] [50] and linear discriminant analysis (LDA) are typically used for feature extraction and classification [51] [42] [52], which is optimal for this study. While all these approaches were considered, LDA was selected for peak classification due to its ability to rigorously separate two classes by features, such as peak current and potential, thus separating the analyte from interfering amino acids. Though both LDA and SVM are suitable for this task, LDA provides a more straightforward and effective solution for resolving overlapping peaks in this application by effortlessly multiplying the features with the LDA eigenvalues to classify the peaks [53].

This paper primarily focuses on developing novel techniques for the data analysis aspect of TDM. These approaches aim to address the challenges of changes in pH and interference substances in sweat, making them applicable to running on wearables for TDM. Traditionally, innovation is applied to the electrodes through chemical developments. In this paper, the focus is on the data analysis aspect. The shift in focus, composed of intelligent algorithms containing machine learning approaches applicable to the wearable, shows promising results in improving the development of low-cost systems.

This paper first presents the experimental section. Then, the results are discussed, including the smart algorithms to compensate for pH and remove interferences present in sweat. These algorithms are validated in the following section with sweat, and in the next section, they are implemented on a wearable system to demonstrate their potential for real-world applications. The final section provides conclusions.

4.2 Experimental Section

Reagents and Materials

Methotrexate disodium (MTX) (99.35 % purity) was purchased from Haihang Industry Co., (Shandong, China), and L-tryptophan was purchased from (Pharmacia & Upjohn Company, United States). The solutions were created using double-deionised water (18.2 MΩ/cm) (Milli-Q, Merck Millipore).

A phosphate-buffered saline (PBS) solution at pH 7.4 was prepared with potassium chloride and potassium phosphate from Sigma-Aldrich (Belgium), and Britton–Robinson buffer (20 mM) with pH levels of 2 to 8 were prepared with sodium borate, sodium acetate and sodium phosphate from Sigma-Aldrich (Belgium). 100 mM potassium chloride was added. The pH of the buffer solution was adjusted to the desired level using potassium hydroxide and hydrochloride solutions. The pH was measured with a pH meter (914 pH/Conductometer, model 2.914.0020, Metrohm, Herisau, Switzerland).

Voltammetry measurements were performed, and the sweat sample pH was measured (potentiometry) with custom-made screen-printed electrodes containing carbon (C2030519P4) working and counter electrodes and silver/silver chloride reference electrodes (C2040308P2) of Sun Chemical, United States. Polyethylene terephthalate (PET, 125 μm) was used as

a substrate. For the pH measurement, the electrodes are modified with aniline and HCl (Sigma-Aldrich, Belgium) following the protocol as described in previous work [54].

The sweat samples were provided by a healthy volunteers (male and female, 30-65 years old) during a regular 1.5 h outdoor running exercise. The skin was cleaned with deionised water and the sweat was collected using an absorbent patch (Cutisoft, BSN Medical, The Netherlands, collection area: 25 cm^2) that was covered with Parafilm (Sigma-Aldrich, Belgium) and attached to the skin at the medial lower back with Fixomull (BSN Medical, The Netherlands). The sweat was extracted from the absorbent with a 5 ml syringe and stored at -18 °C. Sweat tests were approved by the Human Ethics Research Committee of Delft University of Technology.

Instrumentation and Apparatus

Voltammetry and potentiometry were conducted using a MultiPalmSens4 and EmStat4R potentiostat (PalmSens, The Netherlands). Square wave voltammetry was performed within a potential range of -0.1 to 1.5 V, with a step potential of 5 mV, an amplitude of 25 mV, and a frequency of 10 Hz. The voltammetric measurements in buffers described in this manuscript contained 100 mM KCl solution.

Electrochemical Analysis

Matlab was utilised to analyse the data and develop the algorithms (MathWorks, United States).

Wearable System

For this study, a wearable system has been developed. The potentiostat generally consists of a microcontroller controlling a negative feedback and a transimpedance amplifier (TIA) connected with a digital-to-analog converter (DAC) generating the waveforms. The output is fed to an analog-to-digital converter (ADC) to the microcontroller for analysis [8]. This design is reproduced with the following components: STM32L432 microcontroller (STMicroelectronics, Switzerland), ADA4500-2 OPAMP (Analog Devices, United States), DAC70502 DAC (Texas Instruments, United States) and ADS7946 ADC (Texas Instruments, United States) assembled on a PCB and programmed with the STM32CubeIDE (STMicroelectronics, Switzerland). The system outputs the concentration via USB to a serial terminal on the PC.

4.3 Results and Discussion

In the following section the results are presented and discussed.

4.3.1 Voltammetric detection of Methotrexate

First, MTX was interrogated on the SPE by SWV. Figure 4.1A depicts the raw voltammogram of 5 μM MTX exhibiting an increased capacitance current upon increasing voltage. To obtain a clear view of the Faradaic currents occurring during the electrochemical oxidation of MTX, a preprocessing step is needed to enhance the sensing concept's analytical capabilities. Preprocessing the MTX voltammogram consists of applying baseline compensation and

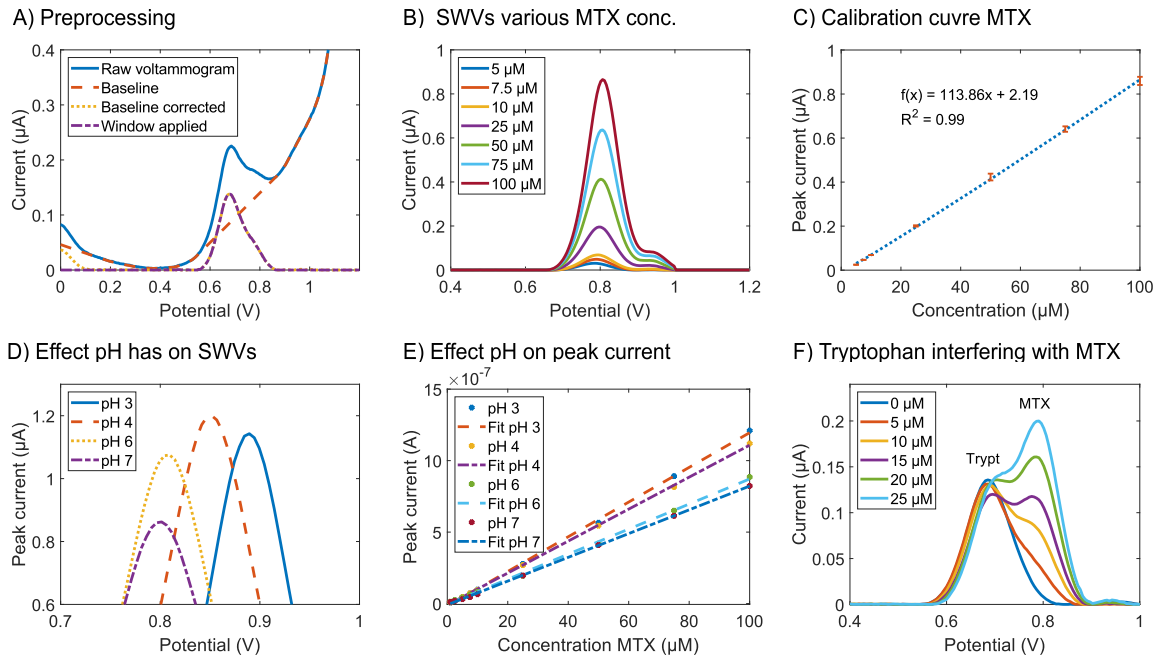

Figure 4.1: Challenges of measuring MTX. A) Pre-processed square wave voltammogram (SWV) of the antineoplastic drug methotrexate, which includes baseline compensation and a detection window. B) SWV of increasing concentrations of MTX. C) The linear relationship of the peak heights of Figure B and the concentration of MTX. D) Effect of pH on the peak potential and current of 100 µM MTX. E) The linear relationship of the peak current and the concentration of MTX at various pH levels. F) Interferent study using 10 µM tryptophan as the main interferent in human sweat with various concentrations of MTX in PBS 7.4 with 0.1 M KCl. The resulting voltammograms highlight the peaks corresponding to both tryptophan and MTX.

applying a window to remove signals at both ends. The baseline compensation removes the background current, which can differ slightly for every measurement. It compares a point in the voltammogram with the average of the two neighboring points. If the average peak is less than the point (for oxidation peaks), it replaces it with the average point. The algorithm stops when no points are updated or until it hits an upper limit [55]. The window targets the redox process link to the analyte, and for MTX, it starts at 0.4 V and stops at 1 V (mean MTX is 0.78 V). The preprocessed voltammogram is then ready for further analysis (Figure 4.1A). The continuous calibration curve of MTX in PBS 7.4 from 5 μM to 100 μM (Figure 4.1B) shows that the peak current of MTX linearly increases according to its rising concentration. This range was chosen because the lowest concentration of MTX that can be reliably measured before the signal-to-noise ratio (SNR) becomes too low is approximately 1 µM. While higher concentrations can be measured effectively and are useful for demonstrating linearity, the maximum concentration of MTX found in sweat during therapeutic drug monitoring is around 3.7 μM (N=5) [32]. Although low concentrations are desirable for actual applications, a compromise was made to address interference from amino acids in sweat. The mean value of the amino acid interference was taken into account, and the lowest MTX concentration that could be effectively isolated was 5 µM (Figure 4.1F). Higher concentrations of MTX

were also measured to illustrate the linear relationship further. Figure 4.1C shows the linear relation between the peak height and the concentration of MTX. The calibration curve using SPEs exhibits a slope of 0.00878 μA/μM, a LOD of 2.13 μM, a LOQ of 6.46 μM and excellent reproducibility of a maximum 4% standard deviation (SD) in peak current (N=3).

The pH of human sweat can dramatically change depending on the physiological conditions of the person. Therefore, it is highly relevant to study the effect of pH on the MTX response as different pH in sweat can significantly affect the MTX measurement. Figure 4.1D shows the peak current and potential shift upon interrogation of 100 µM under different pHs (i.e. pH 3, 4, 6 and 7). The peak potential considerably shifts toward lower potential upon alkaline pHs. When performing a calibration curve at each pH condition, the linear relation between the peak current and the concentration is intact despite the changes in the slope and intercept (Figure 4.1E). The slope and intercept between the varying pH levels have a non-linear relation, which can probably result from the deprotonation of MTX at 5.48 pKa [56], showing the complexity of pH's effects on the voltammogram of MTX.

Another challenge with detecting MTX in sweat is the interference with other substances. The voltammogram of the amino acids tyrosine and tryptophan exhibits reduction–oxidation potentials similar to those of MTX (Figure 4.1B and Figure S1). Changing concentrations of these amino acids in sweat increases the complexity of identifying MTX. For our case study, tryptophan was selected as it is the closed electroactive interferent to the peak potential of MTX. Figure 4.1F shows various concentrations of MTX and 10 µM tryptophan, the average concentration in sweat according to [57]. The amino acid has a slightly lower potential, resulting in MTX showing a peak exiting the tryptophan's voltammogram when the concentration increases. The existing curve is a bell curve, a standard SWV curve with a shoulder on the left. As MTX increases, the peak related to MTX rises and becomes dominant. Thus, interfering substances react heavily with the voltammogram of MTX. An equivalent reaction occurs with tyrosine, but distinguishing it from MTX is more challenging with tryptophan due to tyrosine's lower potential (Figure S1).

4.3.2 Compensation for pH effects

Compensating for pH effects is complex due to the non-linear relationship between the slope of the linear relation between peak current and concentration at different pH levels. The proposed solution uses a lookup table (Figure 4.2A) to extract the appropriate slope for each pH value. This table contains slope values for pH levels ranging from 2 to 8. Values are rounded to the nearest integer for non-integer pH levels that fall outside this range. If the pH level is known, the concentration can be estimated. Additionally, there is a logarithmic relation between the pH and the peak shift (potential) for a constant concentration of MTX (Figure 4.2B, the relation between 10 µM of MTX peak potential and varying pH levels), with a coefficient of determination of 0.97. Unfortunately, the slope and intercept of this line change for different concentrations of MTX, but again, this is a logarithmic relation (Figure 4.2C and 4.2D), with a coefficient of determination of 0.94 and 0.95, respectively. Although the coefficients are not highly accurate, the data clearly shows a linear relationship. However, determining the concentration is the main objective, but using the sheer magnitude of the peak current (Figure 4.2E) to select the slope and intercept and using the peak potential for calculating the pH. The algorithm can then estimate the concentration using the pH and the lookup table, resulting in an algorithm that can overcome deviations in peak current and potential due to varying pH.

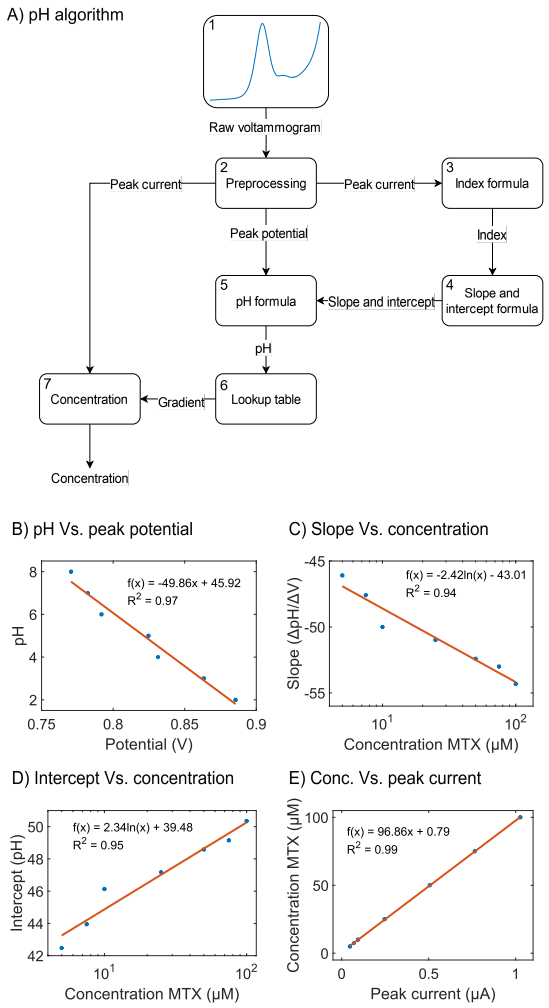

Figure 4.2: pH Algorithm. A) The algorithm determines the concentration using a voltammogram's peak current and peak potential. B) The graph illustrates the relationship (both linear and logarithmic) between pH and the peak potential shift for 10 µM MTX. C and D) Relationship between the slope and intercept with different concentrations of MTX. E) The concentration can be estimated based on the magnitude of the peak current, averaged over the pH range of 2 to 8.

The pH algorithm was tested by analysing the average trends from three SPEs. Measurements from individual electrodes across the entire range were randomly selected (Table 4.1) to verify their accuracy. The raw voltammograms were inserted, and the peak current and potential were extracted for further use in the algorithm. Each measurement's pH and MTX concentration were compared with the algorithm's predicted outcomes. The error was calculated by comparing the desired MTX concentration with the estimated values.

The results indicate that the algorithm's estimation shows more significant error at low concentrations despite minimal differences in the predicted pH. This error is high probably because the signal is more susceptible to background noise. The signal strength is weaker at low concentrations, making the SNR, which compares the desired signal's strength to the

Table 4.1: Results pH algorithm

Measurement	Concentration MTX (µM)	pH	Peak current (nA)	Peak potential (V)	Estimated pH	Predicted concentration MTX (µM)	Error (%)
1	1	4	9.73	0.791	4.55	0.87	13.00
2	2.5	7	25.00	0.766	6.71	2.94	17.60
3	5	8	33.06	0.759	7.38	3.89	22.20
4	7.5	6	78.57	0.789	6.49	7.10	5.33
5	10	3	113.00	0.862	3.25	10.55	5.50
6	25	5	268.00	0.822	5.40	23.96	4.16
7	50	2	582.00	0.894	2.00	50.54	1.08
8	75	5	795.00	0.827	5.10	71.06	5.25
9	100	4	1123.00	0.832	5.15	100.12	0.12

noise level, decreases. When the signal is weak, even small amounts of noise can significantly distort the measurement, making it harder to distinguish between the actual signal and the background noise. As a result, the accuracy of the estimation decreases at lower concentrations. However, the algorithm performs astonishingly at a concentration above 7.5 μM MTX, showing less than 6% errors.

The presented highlight the complexity of compensating for varying pH when estimating the concentration of MTX using SWV. The primary challenge arises from the non-linear relationship between pH and the peak current and potential, which [4] demonstrated for other drugs. However, MTX's relationship between pH and peak potential is highly linear. Unfortunately, when the MTX concentrations change, the slope and intercept of this line (the relation between peak potential and pH) alter logarithmically, as shown in Figures 4.1 C and D. The average of the slope and intercept may be utilised instead, resulting in an error whose concentration is insignificant because the error is mainly comprised of the proper slope. However, looking only at the pH estimation, the algorithm scores 20 % higher estimating the correct pH than using the mean (Table S1). Moreover, selecting the proper slope (Figure S2) is more challenging due to the deprotonation of MTX, which arguably has a type of S-shape; however, this needs further research to be proven and included in the algorithm. Another factor that is highly responsible for the error is the moderate reproducibility of the used SPEs (N=3). Overall, the algorithm performs accurately but could be more robust and effective when increasing (i) the reproducibility of the SPEs and (ii) adding extra data points to validate the algorithm and to improve the accuracy. Regardless, it demonstrates that various relationships can be utilised to reduce errors in some aspects of the measurements.

4.3.3 Peak identification in the presence of interferents

Sweat is an interesting non-invasive matrix rich in physiological information. Sweat can contain levels of therapeutic drugs as well as other biomolecules that can interfere with the sensing of the analyte of interest. First, a research into the state of the art showed that tyrosine and tryptophan are present in sweat at uM levels [57] and oxidation reactions of these substances will potentially interfere with the oxidation of MTX [27]. To verify this assumption, square wave voltammetry was performed with sweat samples obtained from subjects by the adsorbent patch method during the sports exercise (Figure S5). The SWV profile showed redox peaks at 0.716 V and 0.691 V, potentially due to the electro-oxidation of amino acids at the carbon SPE around pH 7.4. To verify this, standards of 50 uM of the possible electroactive

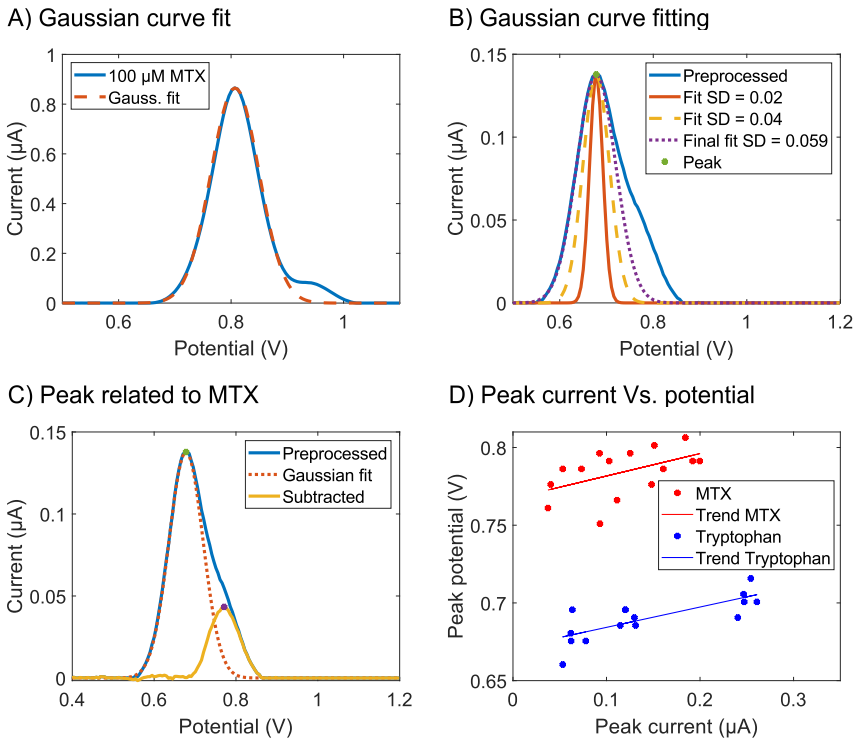

Figure 4.3: Interference Algorithm. A) The voltammograms of 100 μM MTX in PBS at pH 7.4 with 0.1 M KCl show that it fits perfectly a Gaussian function. B) Gaussian fit procedure of 10 μM Tryptophan and 5 μM MTX at pH 7.4 with 0.1 M KCl. C) Fitted Gaussian and the curve related to 5 μM MTX, which is the Gaussian subtracted from the pre-processed voltammogram. D) The peak location of the peaks related to MTX and tryptophan.

interferents (tryptophan, methionine, tyrosine, histidine, cysteine, proline, ascorbic acid, uric acid) in ACE 5 were analysed with the SPE. Figure S1 shows that ascorbic acid, uric acid, tryptophan and tyrosine showed prominent peaks in the recorded potential window. Tryptophan and Tyrosine showed peaks (at 0.77 V and 0.75 V) that overlap with the peak potential window of MTX at pH 7.4 (mean 0.78 V from 1 to 100 μM). Additionally, tryptophan and tyrosine were mixed with MTX to assess their interference in PBS at pH 7.4 (Figure S1B), revealing significant overlap with MTX. To evaluate the potential interferences found in sweat in the analysis of MTX a tailored algorithm was explored. Figure 4.1F shows the SWV of tryptophan with MTX, resulting in an overlapping signal with two peaks or a shoulder. An approach to detect the shoulder can be by differentiating the voltammogram once or twice (Figure S3). The resulting shoulder height identified by the derivative can be used to estimate the MTX concentration. Another method is to fit a Gaussian curve. An algorithm is developed to fit a Gaussian curve on SWVs of varying tryptophan concentrations and identify the MTX concentration. Figure 4.3A shows that 100 μM MTX nearly flawlessly fits a Gaussian curve. The Gaussian formula consists of the curve's amplitude, shift, and width. Figure 4.3B shows the procedure for fitting a Gaussian curve on a signal. First, the dominant peak is located for the amplitude and shift for the curve fitting. Secondly, the width or standard deviation of the Gaussian is increased during iterations until it reaches the boundary of the signal. Third, the curve is subtracted from the signal, resulting in a curve related to the

Table 4.2: Results interference algorithm

Concentration Tryptophan (µM)	Concentration MTX (µM)	SPE A	SPE B	SPE C	SD	Mean	Error (%)
5	5	6.19	7.36	7.40	1.19	6.99	39.70
	10	12.99	12.55	13.86	1.84	13.13	31.33
	15	14.94	14.69	14.95	0.11	14.86	0.92
	20	19.35	19.29	18.92	0.48	19.19	4.07
	25	23.98	25.01	23.44	0.62	24.14	3.43
10	5	7.22	7.12	7.77	1.38	7.37	47.43
	10	10.44	10.57	10.71	0.34	10.58	5.76
	15	15.66	13.79	12.41	0.98	13.95	6.98
	20	20.35	20.69	20.73	0.35	20.59	2.95
	25	25.00	25.20	24.76	0.11	24.98	0.06
20	5	7.47	9.37	10.83	2.56	9.22	84.42
	10	14.93	12.03	14.31	2.28	13.76	37.55
	15	17.52	17.97	14.05	1.34	16.51	10.07
	20	23.18	21.83	15.98	1.81	20.33	1.65
	25	33.21	27.07	20.25	3.24	26.84	7.37
15	5	7.65	8.94	8.86	2.04	8.48	69.59
5	15	16.36	16.69	16.64	0.91	16.56	10.42
7.5	7.5	8.72	9.61	10.18	1.21	9.50	26.72
15	15	16.29	17.62	18.09	1.42	17.33	15.56
20	25	25.76	27.52	26.69	1.04	26.66	6.64

MTX concentration. The peak height of the related MTX curve gives a valid estimation of the MTX concentration. The last part of the procedure is to identify the peak of MTX with linear discriminant analysis (LDA).

LDA is a machine-learning algorithm that maximises the ratio of overall variance to within-class variance to expand the separation between classes. In the training data, tryptophan and MTX are the classes, and the peak currents and potentials are the features. The peak potential is an applicable parameter because MTX has a higher peak potential than tryptophan and tyrosine. However, increasing concentrations in both MTX and tryptophan show a rising trend in both the peak current and peak potential. (Figure 4.1B). The peak current can, therefore, be utilised to increase the spread between MTX and tryptophan (Figure 1D). Moreover, LDA uses the between-class variance, the same as the covariance of the data set whose members are the mean vectors of each class, and the mean sum of the classes' covariance matrices. LDA divides these matrices to maximise the separation [53]. Projecting the data onto the significant eigenvector of the new matrix divides the data (Figure S4). New data is multiplied with this vector to classify it as MTX or tryptophan.

The interference algorithm is applied to the measurements of three SPEs varying in MTX and tryptophan. The tryptophan range is according to the concentrations in sweat [57]. The LDA algorithm is trained on the mean values from the first 15 measurements. After that, it is applied to the individual electrodes and shows 100 % accuracy in identifying MTX. To validate the algorithm, a verification set is made (the last five measurements in Table 4.2), where the algorithm can successfully separate and identify the MTX-related peaks. The algorithm uses the coefficients of the linear equation of Figure 4.1C to transform the peak currents to concentration MTX.

The Gaussian fitting algorithm is inherently complex. The other approach, which uses derivative(s) to identify the shoulder, introduces additional challenges as well, mainly due to

the increased noise in both the first and second derivatives. Developing an algorithm that first smooths the signal before locating the shoulder, especially in the presence of multiple local minima and maxima, further complicates the process. After smoothing, the derivative is applied to identify the peak or shoulder height related to MTX. Hereafter, the concentration of MTX can be calculated using the coefficients of the linear equation shown in Figure 4.1C. However, a challenge arises when dealing with low MTX concentrations (e.g. 5 μM) and high tryptophan concentrations (e.g. 15 μM), where the shoulder may not be detected due to the derivative showing no local minima or maxima, probably due to a low SNR. For the Gaussian fit (Table 4.2), the error is generally for low concentrations MTX and high concentrations tryptophan incorrect, similar to the problems the derivative detection faces. However, the error in this approach is significantly higher than the Gaussian fit algorithm, underscoring the exactness of the latter (Table S2).

Overall, the Gaussian fit algorithm proved to work when peaks overlap, and a shoulder is perceptible or when there are two peaks. It shows excellent results with low error at higher concentrations. Nevertheless, the deviation between reproducibility between the electrodes is significant, which also results in occasional higher average error. It also performs better than the more straightforward derivate approach. However, further research is required for concentrations lower than 5 μM MTX, usually found in sweat. Additionally, changing the pH affects the peak potential (Figure 4.1D pH effects). In this study, the results are obtained from tryptophan and MTX at pH 7.4. Unfortunately, for tryptophan, peak potential shift due to pH does not have a similar relation as that of MTX, resulting in perfectly aligned peaks around pH 6 (Figure S6). The algorithm cannot differentiate between the two, and other techniques should be employed. A possible solution is to use a buffer reservoir to change the pH of the sweat before applying electrochemical analysis, similar to the method described in literature [54].

4.3.4 Validation with sweat samples

Sweat was spiked with MTX to validate the algorithms. First, the voltammogram is preprocessed. Second, the Gaussian fitting algorithm extracts the MTX-related peak. Last, the pH algorithm estimates the pH from the peak potential and uses this to select the proper slope to calculate the MTX concentration. Figure 4.4A shows a sweat sample with pH 7.35 and 5 μM MTX. Figures 4.4B and C show the same sweat sample spiked with 10 μM MTX spiked but with different electrodes. Finally, in Figure 4.4D, 10 μM MTX was spiked in another sweat sample. The sweat samples had slightly different pH levels, 7.35 and 7.51. Nevertheless, the figures show a similar curve to the solution with tryptophan and MTX in buffer, including an MTX-related shoulder.

The Gaussian algorithm effectively fits a Gaussian curve to the signal, subtracting it to isolate the MTX-related peak, which LDA accurately identifies across all four figures. However, the fit indicates that the sweat sample deviates slightly from an ideal Gaussian curve compared to the buffer, probably due to other components in sweat, such as tyrosine, which has a lower peak potential. Despite this variation, the MTX-related peak height is according to the peak height in the buffer. Following the Gaussian fit, the pH algorithm is employed, estimating pH values of 7, 7, 8, and 8, respectively. It then calculates the MTX concentrations as 5.02, 7.66, 11.19, and 9.36 µM, demonstrating the algorithm's potential. Although this is relatively accurate for these samples, sweat varies, such as in NaCl, which deviates between 10 and 90 mM [38] [58], shifting the peak potential according to the Nernst equation (Figure

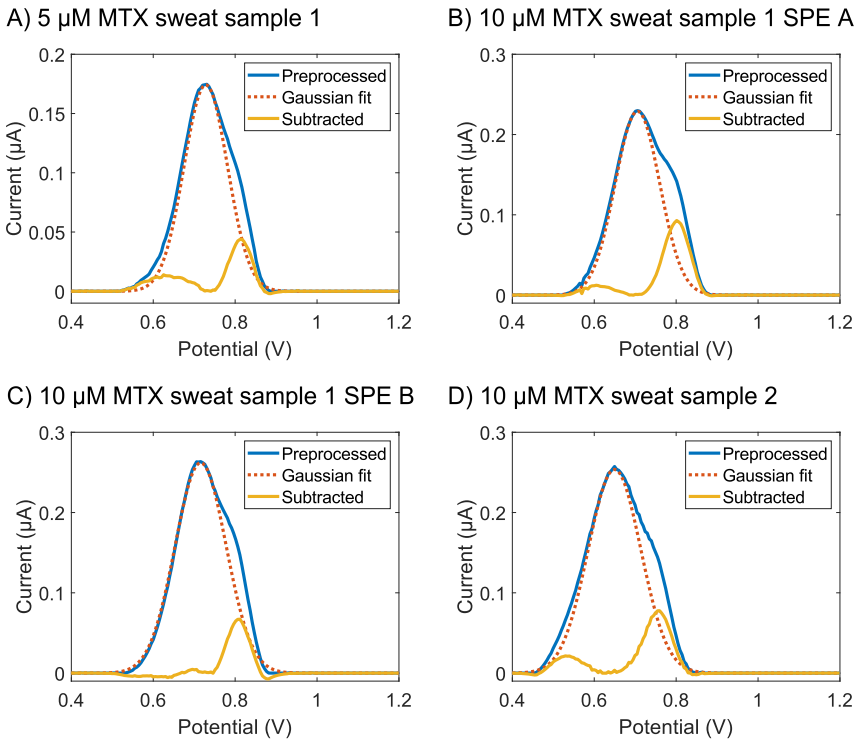

Figure 4.4: Validation of the algorithm using sweat samples. A) Voltammogram of sweat sample 1 spiked with 5 μM MTX. B and C) Voltammograms from different electrodes of sweat sample 1 spiked with 10 μM MTX. D) Voltammogram of sweat sample 2 spiked with 10 μM MTX.

S7). This results in the pH algorithm not effectively estimating the concentration. Further, the peak height can vary significantly, which, in addition to other factors, may be caused by temperature fluctuations (Figure S8). Further research is necessary to enhance the algorithm's robustness across diverse sweat samples and refine its accuracy, mainly due to physiological and environmental variations.

4.3.5 Implementation on wearable

The voltammogram of sweat sample 1 SPE A, spiked with 10 μM MTX, has been uploaded to the Wearable (Figure S9). The wearable device has been specially developed for this research to show how achievable the algorithms are if executed on a small, low-power microprocessor. Usually, the Wearable performs an SWV, whereafter the algorithms compute the molar concentration and output it via USB to a serial monitor; however, the sweat sample voltammogram is uploaded to the Wearable for validation. The Wearable executes the baseline compensation, a relatively intensive algorithm that goes through the voltammogram several 100 times to remove the baseline. Second, a window is applied to remove other possible interferences; whereafter, the peak current is obtained. Together with the peak potential, they are required for the Gaussian fit algorithm that removes the influence of amino acids and leaves over a peak related to the MTX concentration. At last, the pH algorithm compensates for the pH shift (Figure S10).

The result is that the algorithm estimates the pH at 6.2 and the concentration at 9.26 μM, which differs from the algorithms implemented in MatLab. Presumably, there is some loss due to the conversions in data for the microcontroller and the calculation of the algorithms with it, which needs further optimisations. Nevertheless, the estimated concentration is still reasonably accurate, and the Wearable performs all the algorithms in less than 200 milliseconds at 80 MHz. These results demonstrate that the algorithms can be effectively executed on an embedded system, enabling real-time sweat analysis. This indicates significant progress in developing wearable sensors for therapeutic drug monitoring.

4.4 Conclusion

In conclusion, this paper has demonstrated several approaches to overcoming challenges in Therapeutic Drug Monitoring (TDM). The focus was on developing intelligent algorithms to compensate for pH variations and remove components that interfere with electrochemical measurements. These algorithms can run on wearable systems and improve exactness and affordability. The proposed algorithm uses Gaussian fitting and LDA to separate interfering amino acids in sweat to obtain peaks related to the analyte Metrothexate (MTX), which is utilised. The Gaussian fit algorithm effectively separated peaks and identified the peak associated with the analyte. For pH compensation, the pH is estimated using the relation between the peak potential and the pH. The peak height is used together with other relations to increase the algorithm's effectiveness. However, due to low concentrations of drugs found in sweat and utilised in this research, and with limited measurement, challenges occur due to high signal-to-noise ratios and reproducibility. Nevertheless, further research is required to improve the algorithms by extending the data set, further validation and the reproducibility of the SPEs. Overall, the presented approaches are a leap forward in overcoming complex problems in the sweat matrix using intelligent algorithms.

4.5 Supplementary

Supplementary Figure S1

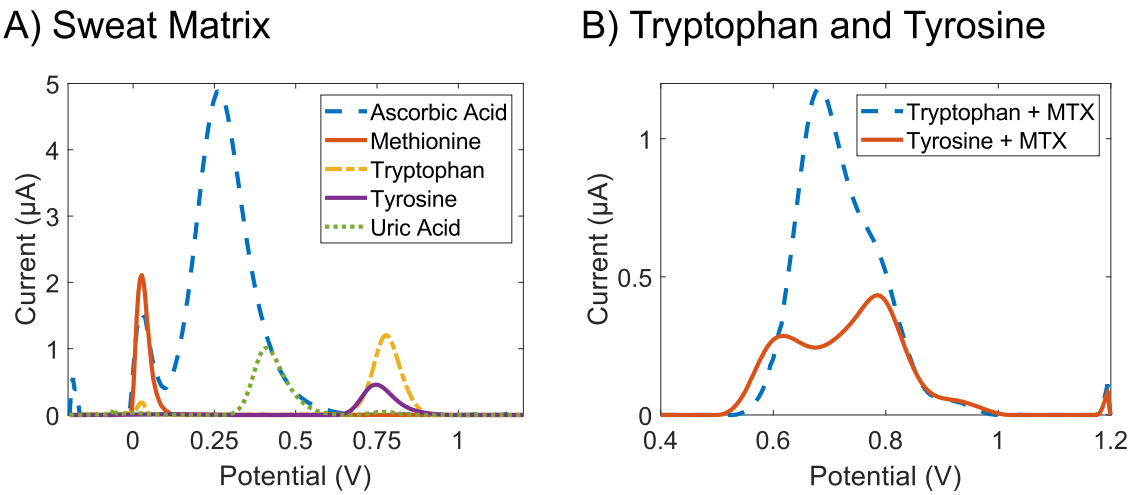

Figure S1: Interference study of substances in the sweat matrix. A) Ascorbic acid, methionine, tryptophan, tyrosine and uric acid show redox reactions when square wave voltammetry is executed in acetate buffer (pH 5) between -0.2 and 1.2 V. Histidine, cysteine, and proline do not exhibit any redox reaction under these conditions. Tryptophan and Tyrosine have a similar redox potential of 0.777 and 0.747 V, respectively. B) Overlap between the redox signals of tryptophan, tyrosine, and MTX phosphate-buffered saline (pH 7.4).

Supplementary Figure S2

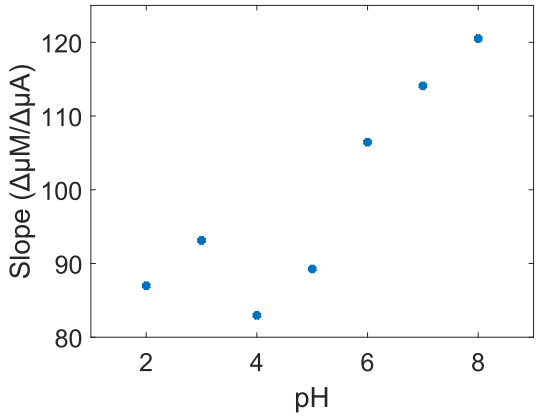

Figure S2: The lookup table of the pH algorithm consists of the continuous calibration slopes of each pH level. The proper slope for each pH can be selected and multiplied with the peak current to get the MTX concentration in μM.

Supplementary Table S1

Table S1: Comparison estimating pH level using two different methods.

	MTX (µM)	pH 2	pH 3	pH 4	pH 5	pH 6	pH 7	pH 8
Algorithm	5	2	3	4	5	6	7	8
	7.5	2	3	4	5	6	7	7
	10	2	3	4	5	6	7	7
	25	2	3	4	5	6	7	7
	50	2	3	4	5	7	7	7
	75	2	3	4	5	7	7	7
	100	2	3	4	5	7	7	7
Mean slope and intercept	5	2	3	5	6	7	7	8
	7.5	2	3	4	5	7	7	8
	10	2	3	4	5	7	7	7
	25	2	3	4	5	6	6	7
	50	2	2	4	5	6	6	7
	75	2	2	3	5	6	6	7
	100	2	2	3	4	6	6	7

Note: Estimated the pH level of the pH algorithm by using the peak current to select the slope and intercept and the peak potential to calculate the pH compared with the mean slope and intercept. Mean of 3 SPEs are used to decrease the table.

Supplementary Figure S3

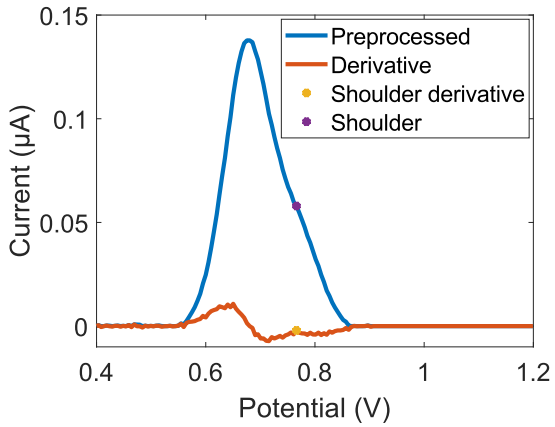

Figure S3: Identify the peak height of the shoulder by using the derivative of the preprocessed curve of 10 μM MTX with 5 μM MTX.

Supplementary Figure S4

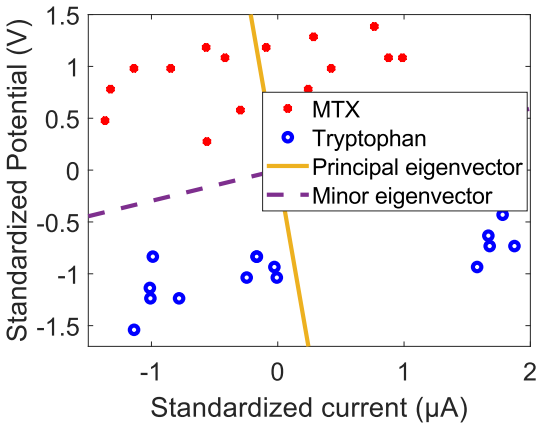

Figure S4: The minor eigenvector and the principle eigenvector on which the data is projected to find the maximum separation between two classes.

Supplementary Table S2

Table S2: Results of identifying MTX from tryptophan using the peak height, which is selected using the derivative.

Concentration Tryptophan (µM)	Concentration MTX (µM)	SPE A	SPE B	SPE C	SD	Mean	Error (%)
5	5	7.88	7.80	10.54	2.28	8.74	74.82
	10	11.41	10.99	12.29	0.95	11.56	15.62
	15	13.37	13.14	13.38	0.99	13.29	11.37
	20	17.77	17.72	17.36	1.38	17.62	11.92
	25	22.42	23.44	21.87	1.45	22.58	9.69
10	5	7.45	7.20	5.61	1.12	6.75	35.05
	10	12.38	10.86	10.52	0.86	11.25	12.54
	15	14.11	14.26	13.74	0.57	14.03	6.44
	20	18.72	19.12	19.12	0.60	18.99	5.07
	25	23.50	23.67	23.25	0.89	23.47	6.12
20	5	8.29	7.84	8.44	1.85	8.19	63.83
	10	15.14	17.08	17.76	3.90	16.66	66.61
	15	20.03	21.43	18.03	2.90	19.83	32.20
	20	24.92	25.82	20.15	2.54	23.63	18.15
	25	31.66	28.99	27.25	2.70	29.30	17.20
15	5		7.47		2.50	7.47	49.36
5	15	14.78	15.12	15.11	0.09	15.01	0.04
7.5	7.5	8.93	9.51	10.06	1.19	9.50	26.66
15	15	17.89	19.24	18.87	2.14	18.67	24.44
20	25	28.45	30.19	29.17	2.50	29.27	17.08

Supplementary Figure S5

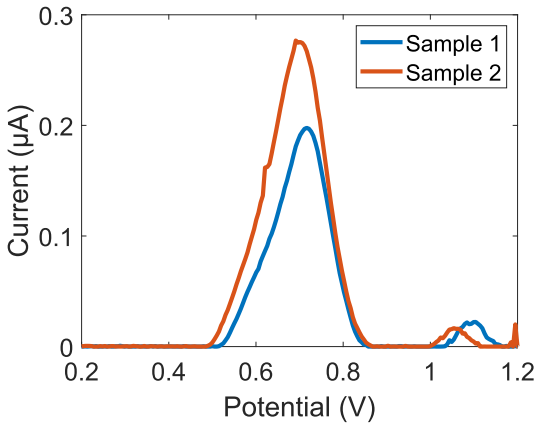

Figure S5: The blank sweat samples of two different volunteers. The peak potential lay at 0.716 and 0.691, respectively.

Supplementary Figure S6

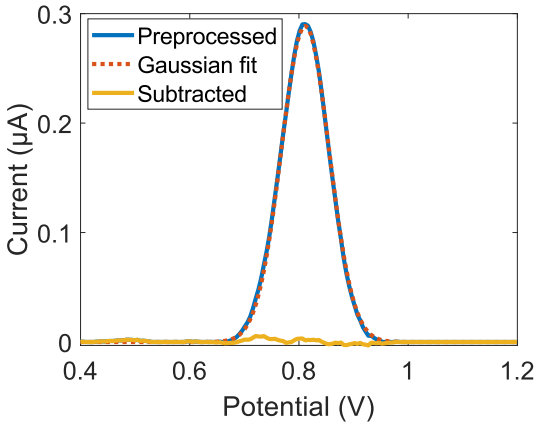

Figure S6: Gaussian fit algorithm applied on sweat sample with a pH of 6.32 containing 5 μM MTX and 5 μM tryptophan.

Supplementary Figure S7

The increasing concentration of NaCl increases the peak potential by roughly 50 mV, according to the Nernst equation.

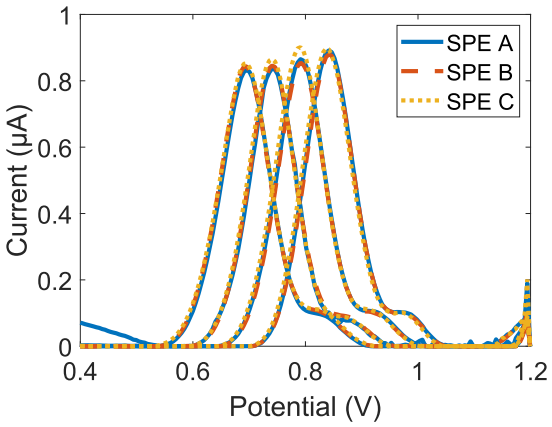

Figure S7: Square wave voltammograms of 100 μM MTX with various concentrations of NaCl (1 mM, 10 mM, 100 mM, and 1000 mM) at pH 7.4.

Supplementary Figure S8

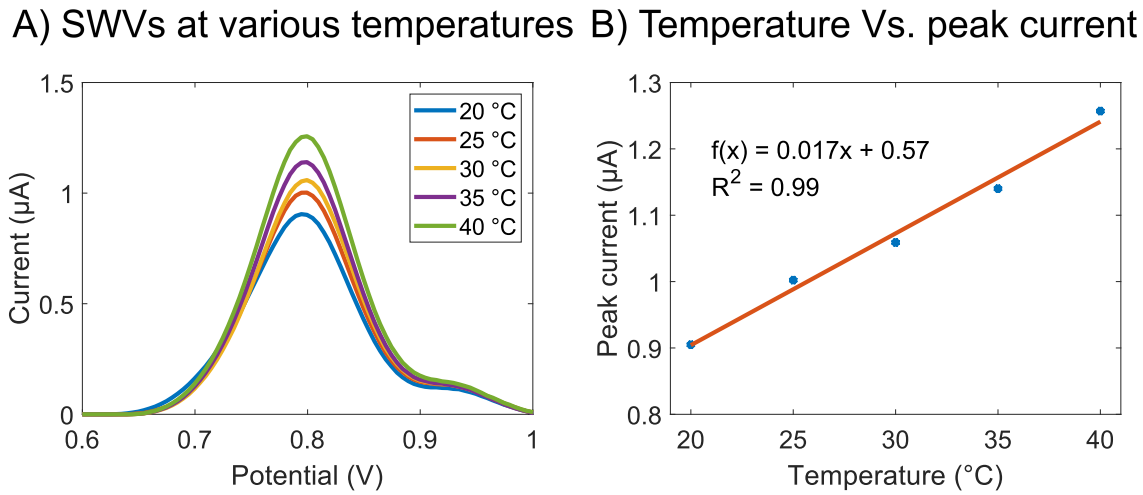

Figure S8: Temperature response MTX. A) Square wave voltammograms of 100 μM MTX at different temperatures at pH 7.4. An increase in temperature increases the peak current. B) Relation between the peak current of 100 μM MTX at various temperatures.

Supplementary Figure S9

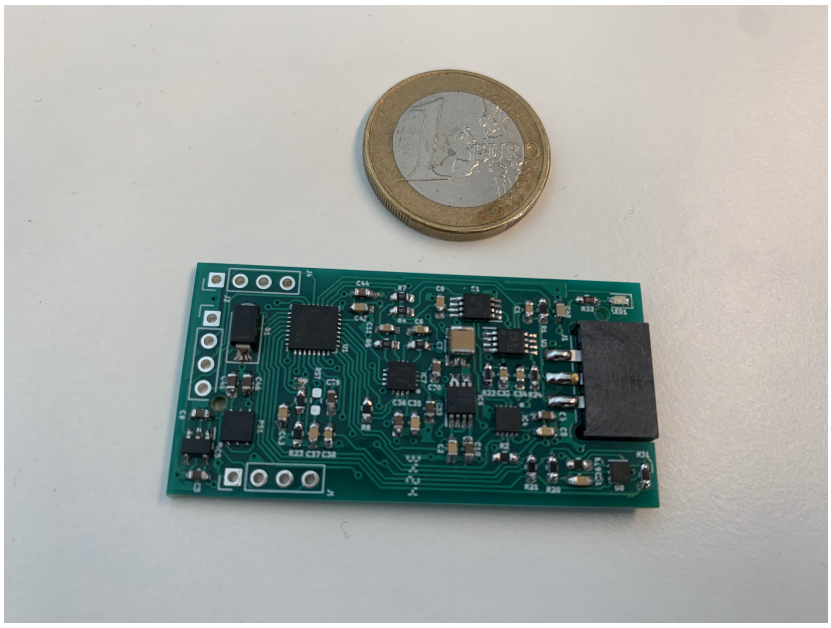

Figure S9: The wearable device shown with a 1 euro coin for size reference.

Supplementary Figure S10

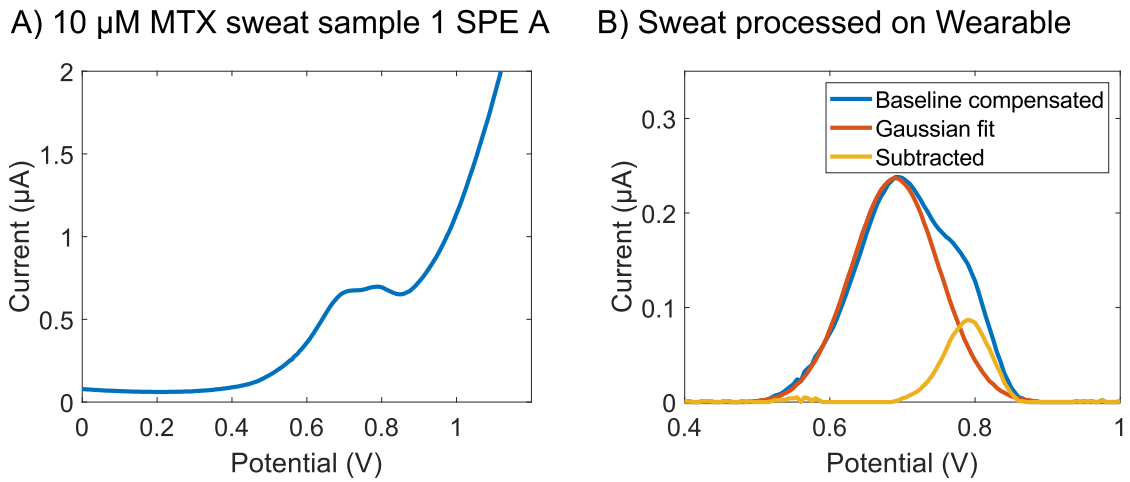

Figure S10: Sweat processed on the Wearable: A) Sweat sample 1 SPE A, spiked with 10 μM MTX. B) The wearable device performed baseline compensation and applied a window, Gaussian fit, and pH algorithm to the uploaded sweat sample, resulting in an estimated pH of 7 and an MTX concentration of 10 μM.

Chapter 5

Conclusion

This project aimed to develop a wearable electrochemical system to improve sweat analysis for therapeutic drug monitoring (TDM). The use case was detecting methotrexate (MTX), an antineoplastic agent, in sweat by using voltammetry, a technique of reducing and oxidising by changing the potential and measuring the related current. However, the sweat matrix influences the measurements due to changes in pH and temperature and in biomarkers that overlap with the wanted signal. A multichannel potentiostat prototype was realised for exploration and testing to improve the measuring system and find new features to benefit the overall analysis. Recommendations to improve the prototype include optimising the code and moving the temperature sensor so that other components less influence it.

The scope of this thesis was confined to developing two novel algorithms that can be executed on a wearable embedded system to compensate for the amino acid tryptophan found in sweat, which overlaps the analyte in sweat, and the effect on the voltammetric measurement of MTX from the change in pH found in sweat (ranging from 2 to 8). The first algorithm uses the relation between the peak potential and pH and the peak current magnitude to refine the estimation of the MTX concentration at varying pH levels, though it requires further validation. A second algorithm was developed that successfully removed tryptophan from MTX by fitting a Gaussian function and identifying the related MTX peak using linear discriminant analysis (LDA).

The algorithms were verified with actual sweat samples. First, the Gaussian fit algorithm extracted the MTX peak, and then the pH algorithm compensated the estimated concentration. While limitations remain, such as overlapping analyte and amino acid signals at lower pH levels and high variability in the reproducibility of screen-printed electrodes (SPEs), the algorithms successfully performed in real-time on the wearable device. Despite challenges in improving detection accuracy at lower MTX concentrations representative of real sweat, the system exhibited promising results.

In conclusion, the wearable system and the algorithms presented in this thesis represent a significant step toward realising real-time, non-invasive TDM via intelligent algorithms that can be executed on a wearable embedded system.

Appendix A

Screen-printed electrodes characterisation

The characterisation of screen-printed electrodes (SPEs) is critical in ensuring the reproducibility of electrochemical measurements. However, significant differences in peak current between electrodes were recorded, even though the measurements were performed simultaneously by applying the same volume from a single solution. Perhaps this can be characterised electronically, which is the aim of this sub-study. Hereafter, the electrodes could be calibrated to improve the reproducibility.

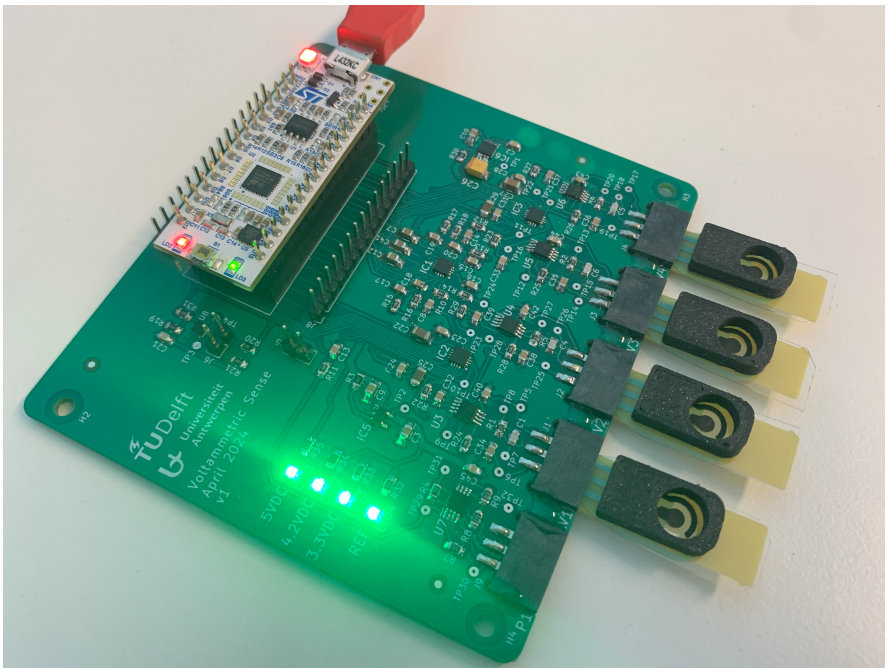

Figure A1: The prototype with four screen-printed electrodes and 3D-printed rings for confining the droplet's height.

The method applied is square wave voltammetry with a droplet of 0.8 μl around the 0.3 mg/ml APAP in PBS buffer with 0.1 M KCl on four SPEs. The droplet's height is confined using a 3D-printed ring mounted on the SPE by double-sided tape (Figure A2). APAP

is chosen for this test due to its lower toxicity than MTX and excellent availability. The prototype applied SWV and increased the potential from -0.5 to 1.2 V with a step size of 0.005 V and an amplitude of 0.025 V at 10 Hz (Figure A2). The peaks are approximately 0.4 V, at 0.219, 0.201, 0.204, and 0.279 μA, respectively, representing the desired potential and current [35]. The difference in peak height of the maximum variation of 28% is significant.

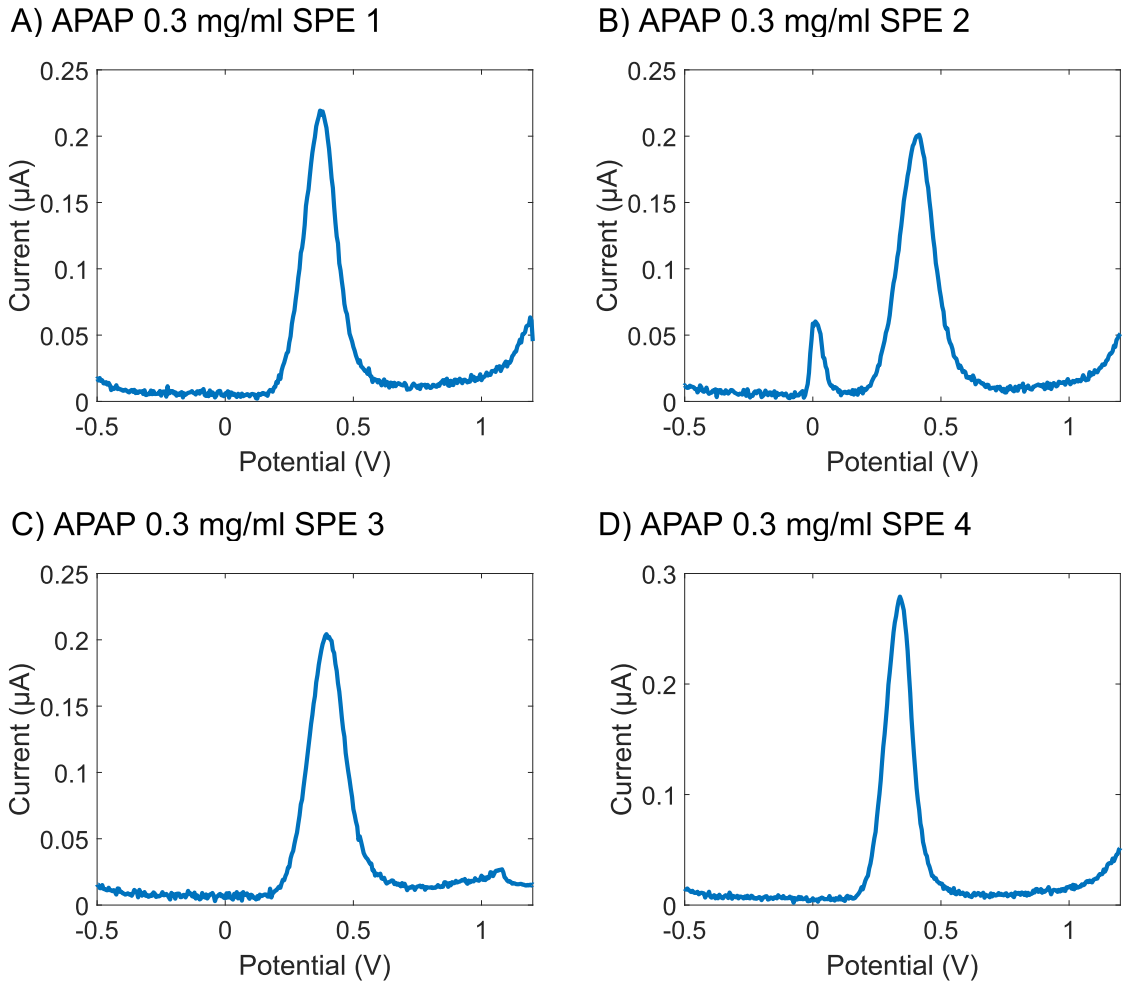

Figure A2: Square wave voltammograms of four different screen-printed electrodes with 0.3 mg/ml APAP in PBS 7.4 with 0.1 KCl.

The initial assumption is that there might be a relation between the peak current and the conductivity. The Randles-Sevcik equation shows that the electrode surface area is part of the equation [7], which is also the case for electrical conductivity. The conductivity can then be measured, with an impedance analyser, between the counter and working, where the reaction happens, and compared with the peak current of an electrochemical measurement for the four SPEs. Hopefully, a relation can be found to characterize and eventually calibrate the electrodes. In table A1, the results of this research are shown. It includes the peak currents, the impedances and the peak potentials.

Unfortunately, there is no relation between the peak current and the impedance or the peak potential and the impedance. Although the measurements were conducted with the utmost

Table A1: The impedance, peak current, and potential of four different electrodes with 0.3 mg/ml APAP in PBS with 0.1 KCl.

SPE	Z	Peak current (µA)	Peak potential (V)
1	822.74	0.2193	0.37
2	917.70	0.2012	0.41
3	825.31	0.2043	0.39
4	868.22	0.2791	0.34

precision, some deviations may have influenced the results. Therefore, further research is needed to determine how to increase the reproducibility of the electrodes. One potential solution is to optimise the production process of the screen-printed electrodes instead of exclusively relying on electronic calibration. Since SPEs are low-cost and fabricated in-house, optimizing the manufacturing process could offer a more effective and economical approach to enhancing performance.

Appendix B

Overlapping voltammogram

The voltammogram of a sweat sample of pH 6 spiked with MTX (Figure S6) or MTX with tryptophan in a buffer with pH 6 shows similar results (Figure A3); the voltammogram is shifted, but the amino acid and MTX do not exhibit the same shift characteristics. The peaks overlap, and the Gaussian fit algorithm to extract the MTX-related peak is ineffective. However, this sub-study aims to solve it using an observed property of amino acids such as tryptophan and tyrosine: they are not repeatable, and the peak decays after each cycle. By utilising this property, it may be possible to obtain the MTX-related peak at pH 6, and with the addition of this to the Gaussian fit algorithm, it can then be performed for the entire pH range of 2 to 8 found in sweat

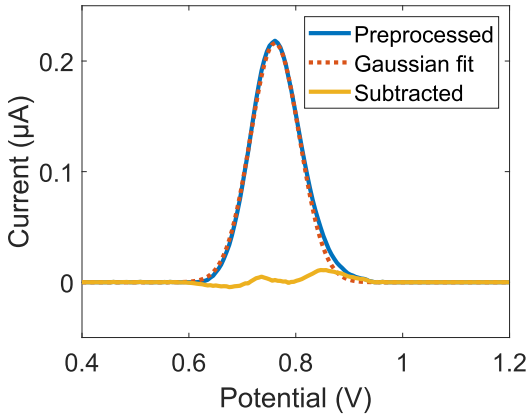

Figure A3: Voltammogram of 5 μM MTX and 15 μM Tryptophan at pH 6.

The assumption is that using various concentrations of MTX and tyrosine or tryptophan and performing several voltammograms while mixing the solution (to overcome mass transport [7]), the decay in the peak can be calculated for the various concentrations and used to determine the concentration of MTX. Figure A4 shows the decay of tyrosine after 5 repetitions for 40 and 60 μM. A power function can be fitted on the peaks of both graphs, with both having a coefficient of determination of 0.99. Unfortunately, the function of $f(x) = Ax^{-B}$ has different coefficients for both coefficients; the B coefficient even shifts with 35%. It was promising if only the A coefficient changes due to the different concentrations and the B coefficient keeps a constant value, which will help decode if MTX is added. Furthermore, this

was also the case for more measurements.

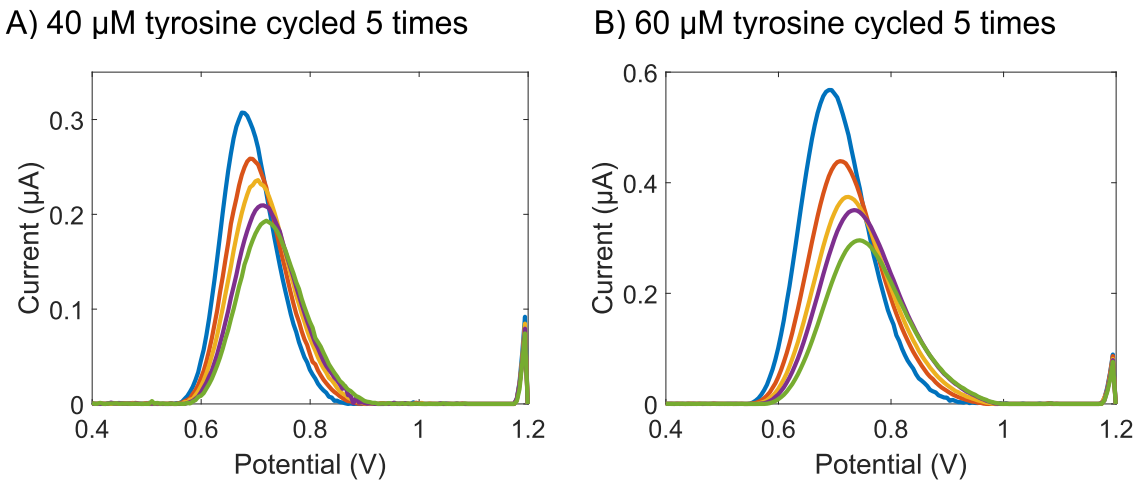

Figure A4: The voltammograms of 40 and 60 μM tyrosine cycled 5 times. The decay is related to a power function.

Finally, the significantly varying coefficients disprove this assumption. Perhaps this is due to the electrode's reproducibility or to inconsistency in the measurement. Nonetheless, a different method should be applied to overcome overlap in peaks at pH 6.

Appendix C

Schematics and PCB design of the Prototype

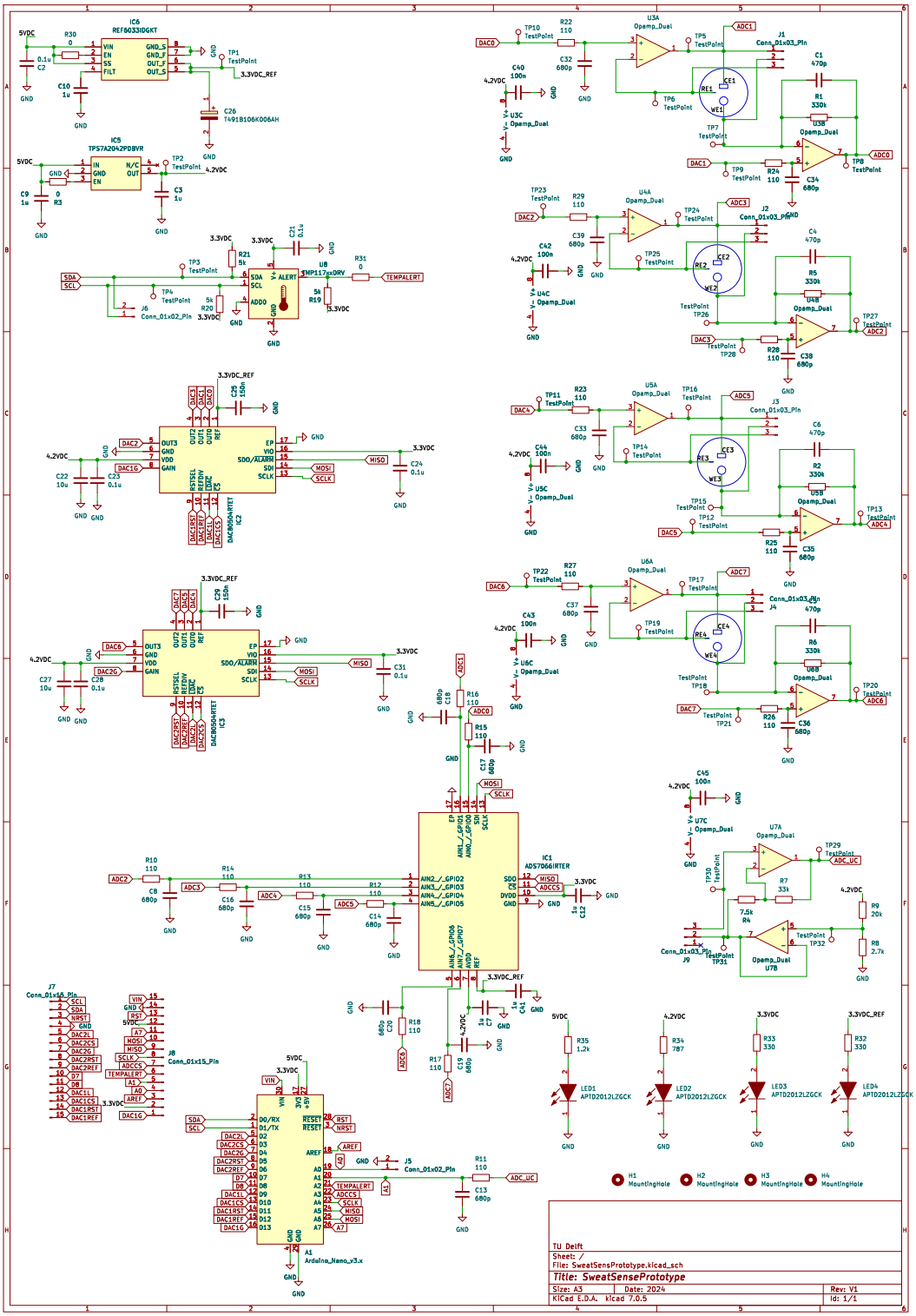

Figure A5: The schematic of the prototype.

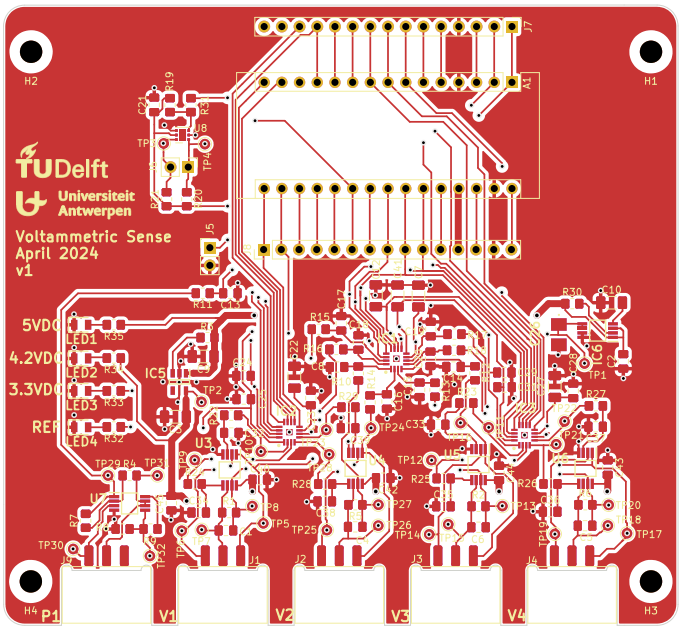

(a)

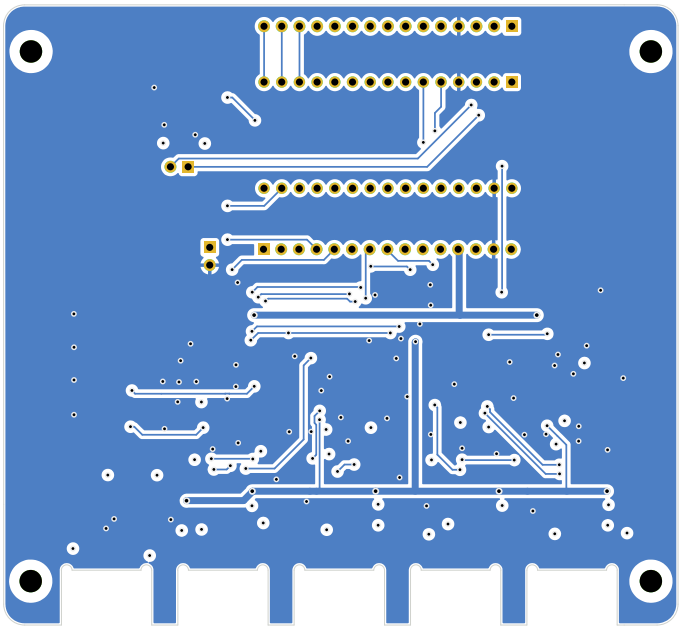

(b)

Figure A6: The design of the printed circuit board (PCB). In (a) the top part and in (b) the bottom part of the PCB.

Appendix D

PCB design of the Wearable

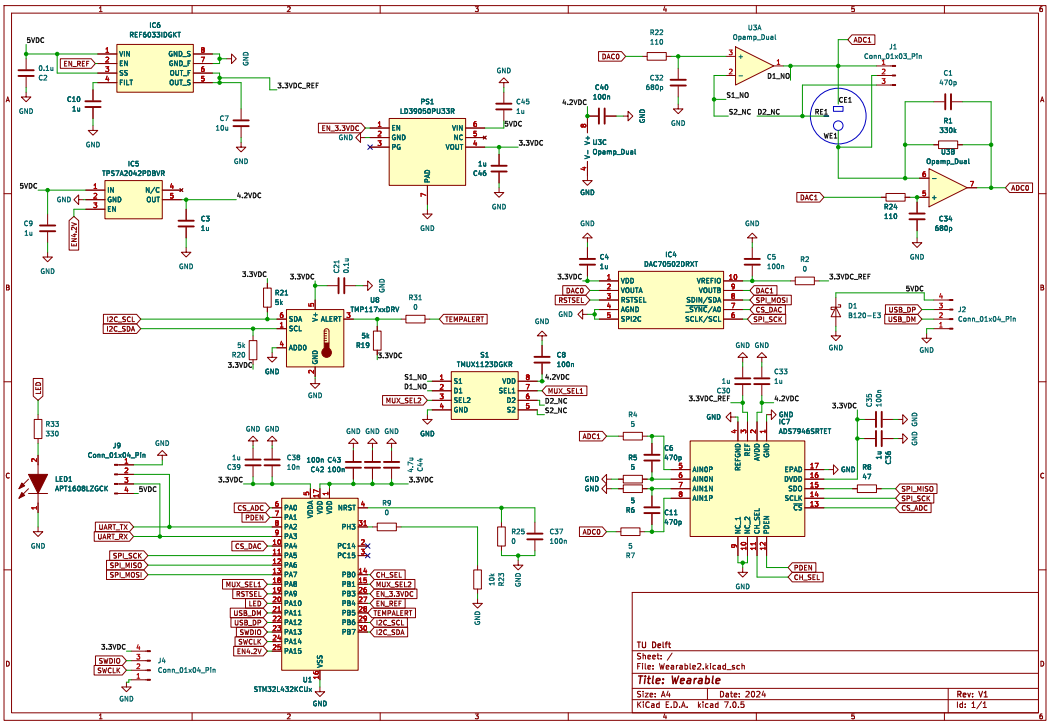

Figure A7: The schematic of the wearable.

Bibliography

[1] Amitava Dasgupta. "Introduction to therapeutic drug monitoring: Frequently and less frequently monitored drugs". In: *Therapeutic drug monitoring*. Elsevier, 2024, pp. 1–35.

[2] Elain Fu et al. "Progress on Electrochemical Sensing of Pharmaceutical Drugs in Complex Biofluids". In: *Chemosensors* 11.8 (2023), p. 467.

[3] Fupeng Gao et al. "Wearable and flexible electrochemical sensors for sweat analysis: A review". In: *Microsystems & Nanoengineering* 9.1 (2023), p. 1.

[4] Paulo A Raymundo-Pereira et al. "Wearable glove-embedded sensors for therapeutic drug monitoring in sweat for personalized medicine". In: *Chemical Engineering Journal* 435 (2022), p. 135047.

[5] Bhavik A Patel. *Electrochemistry for bioanalysis*. Elsevier, 2021.

[6] Rahul M Kotkar, Purvi B Desai, and Ashwini K Srivastava. "Behavior of riboflavin on plain carbon paste and aza macrocycles based chemically modified electrodes". In: *Sensors and Actuators B: Chemical* 124.1 (2007), pp. 90–98.

[7] Noémie Elgrishi et al. "A practical beginner's guide to cyclic voltammetry". In: *Journal of chemical education* 95.2 (2018), pp. 197–206.

[8] Li-Chia Tai et al. "Methylxanthine drug monitoring with wearable sweat sensors". In: *Advanced Materials* 30.23 (2018), p. 1707442.

[9] Somayeh Tajik et al. "Simultaneous and selective electrochemical sensing of methotrexate and folic acid in biological fluids and pharmaceutical samples using Fe3O4/ppy/Pd nanocomposite modified screen printed graphite electrode". In: *Chemosphere* 291 (2022), p. 132736.

[10] Lin Gao et al. "Anodic voltammetric behaviors of methotrexate at a glassy carbon electrode and its determination in spiked human urine". In: *Journal of Electroanalytical Chemistry* 610.2 (2007), pp. 131–136.

[11] Kan Kan Yeung et al. "Recent advances in electrochemical sensors for wearable sweat monitoring: A review". In: *IEEE Sensors Journal* 21.13 (2021), pp. 14522–14539.

[12] Fabio Ruiz Simões and Miguel Gustavo Xavier. "Electrochemical sensors". In: *Nanoscience and its Applications* 1 (2017), pp. 155–178.

[13] Ahmed Barhoum and Zeynep Altintas. *Advanced Sensor Technology: Biomedical, Environmental, and Construction Applications*. Elsevier, 2022.

[14] Philippe Westbroek, Georgios Priniotakis, and Paul Kiekens. *Analytical electrochemistry in textiles*. Elsevier, 2005.

[15] Michael Chung, Giuseppino Fortunato, and Norbert Radacsi. "Wearable flexible sweat sensors for healthcare monitoring: a review". In: *Journal of the Royal Society Interface* 16.159 (2019), p. 20190217.

[16] Hazhir Teymourian et al. "Wearable electrochemical sensors for the monitoring and screening of drugs". In: *ACS sensors* 5.9 (2020), pp. 2679–2700.

[17] Aleksandr B Stefaniak and Christopher J Harvey. "Dissolution of materials in artificial skin surface film liquids". In: *Toxicology in Vitro* 20.8 (2006), pp. 1265–1283.

[18] Hyunjae Lee et al. "A graphene-based electrochemical device with thermoresponsive microneedles for diabetes monitoring and therapy". In: *Nature nanotechnology* 11.6 (2016), pp. 566–572.

[19] Li-Chia Tai et al. "Wearable sweat band for noninvasive levodopa monitoring". In: *Nano letters* 19.9 (2019), pp. 6346–6351.

[20] Wei Gao et al. "Fully integrated wearable sensor arrays for multiplexed in situ perspiration analysis". In: *Nature* 529.7587 (2016), pp. 509–514.

[21] Yiran Yang et al. "A laser-engraved wearable sensor for sensitive detection of uric acid and tyrosine in sweat". In: *Nature biotechnology* 38.2 (2020), pp. 217–224.

[22] Wei Gao et al. "Wearable microsensor array for multiplexed heavy metal monitoring of body fluids". In: *Acs Sensors* 1.7 (2016), pp. 866–874.

[23] Corie Horwood. "Ionic liquids as electrolytes for electrochemistry". In: *Ionic Liquids in Analytical Chemistry*. Elsevier, 2022, pp. 329–342.

[24] O Dominguez Renedo, MA Alonso-Lomillo, and MJ Arcos Martinez. "Recent developments in the field of screen-printed electrodes and their related applications". In: *Talanta* 73.2 (2007), pp. 202–219.

[25] Dana Stan et al. "What is the optimal method for cleaning screen-printed electrodes?" In: *Processes* 10.4 (2022), p. 723.

[26] Raquel García-González et al. "Electrochemical characterization of different screen-printed gold electrodes". In: *Electrochimica Acta* 53.8 (2008), pp. 3242–3249.

[27] Shuyu Lin et al. "Noninvasive wearable electroactive pharmaceutical monitoring for personalized therapeutics". In: *Proceedings of the National Academy of Sciences* 117.32 (2020), pp. 19017–19025.

[28] Yongseok Joseph Hong et al. "Multifunctional wearable system that integrates sweat-based sensing and vital-sign monitoring to estimate pre-/post-exercise glucose levels". In: *Advanced Functional Materials* 28.47 (2018), p. 1805754.

[29] Mallika Bariya, Hnin Yin Yin Nyein, and Ali Javey. "Wearable sweat sensors". In: *Nature Electronics* 1.3 (2018), pp. 160–171.

[30] Dmytro Snizhko et al. "Potentiostat design keys for analytical applications". In: *Journal of Electroanalytical Chemistry* 936 (2023), p. 117380.

[31] *Op Amp Common-Mode Rejection Ratio (CMRR)*. MT-042. Rev. 0. Analog Devices. Nov. 2008.

[32] Robert M Mader et al. "Exposure of oncologic nurses to methotrexate in the treatment of osteosarcoma". In: *Archives of Environmental Health: An International Journal* 51.4 (1996), pp. 310–314.

[33] Palmsens B.V. *Palmsens Multitrace*. Sept. 2024. URL: `https://www.palmsens.com/software/multitrace/`.

[34] Robbert Nederhoff. *Software Prototype and Wearable*. `https://github.com/SweatSens/`. Accessed: 2024-10-02. 2024.

[35] Annemarijn Steijlen et al. *A Practical Guide to Build a Raspberry Pi Pico Based Potentiostat for Educational Electrochemistry and Electronic Instrumentation*. 2024.

[36] Palmsens B.V. *Palmsens MultiPalmSens4*. Sept. 2024. URL: `https://www.palmsens.com/product/multipalmsens4/`.

[37] Ju-Seop Kang and Min-Ho Lee. "Overview of therapeutic drug monitoring". In: *The Korean journal of internal medicine* 24.1 (2009), p. 1.

[38] Lindsay B Baker. "Physiology of sweat gland function: The roles of sweating and sweat composition in human health". In: *Temperature* 6.3 (2019), pp. 211–259.

[39] Udo Hoss et al. "Continuous glucose monitoring in the subcutaneous tissue over a 14-day sensor wear period". In: *Journal of Diabetes Science and Technology* 7.5 (2013), pp. 1210–1219.

[40] Gustavo HG Matsushita et al. "Phasic dopamine release identification using convolutional neural network". In: *Computers in Biology and Medicine* 114 (2019), p. 103466.

[41] Magnus Falk et al. "Wearable Electronic Tongue for Non-Invasive Assessment of Human Sweat". In: *Sensors* 21.21 (2021), p. 7311.

[42] Mousumi Palit et al. "Classification of black tea taste and correlation with tea taster's mark using voltammetric electronic tongue". In: *IEEE Transactions on Instrumentation and Measurement* 59.8 (2009), pp. 2230–2239.

[43] Michael LAV Heien, Michael A Johnson, and R Mark Wightman. "Resolving neurotransmitters detected by fast-scan cyclic voltammetry". In: *Analytical chemistry* 76.19 (2004), pp. 5697–5704.

[44] Michael D Nguyen et al. "Characterization of spontaneous, transient adenosine release in the caudate-putamen and prefrontal cortex". In: *PLoS One* 9.1 (2014), e87165.

[45] Ashley E Ross and B Jill Venton. "Sawhorse waveform voltammetry for selective detection of adenosine, ATP, and hydrogen peroxide". In: *Analytical chemistry* 86.15 (2014), pp. 7486–7493.

[46] Carl J Meunier, Gregory S McCarty, and Leslie A Sombers. "Drift subtraction for fast-scan cyclic voltammetry using double-waveform partial-least-squares regression". In: *Analytical chemistry* 91.11 (2019), pp. 7319–7327.

[47] Cameron S Movassaghi et al. "Simultaneous serotonin and dopamine monitoring across timescales by rapid pulse voltammetry with partial least squares regression". In: *Analytical and Bioanalytical Chemistry* 413 (2021), pp. 6747–6767.

[48] Debangana Das et al. "CuO nanoparticles decorated MIP-based electrode for sensitive determination of gallic acid in green tea". In: *IEEE Sensors Journal* 21.5 (2020), pp. 5687–5694.

[49] Gustavo HG Matsushita et al. "Automatic identification of phasic dopamine release". In: *2018 25th International Conference on Systems, Signals and Image Processing (IWSSIP)*. IEEE. 2018, pp. 1–5.

[50] Jafar Massah and Keyvan Asefpour Vakilian. "An intelligent portable biosensor for fast and accurate nitrate determination using cyclic voltammetry". In: *Biosystems Engineering* 177 (2019), pp. 49–58.

[51] Xiaoyu Zhang et al. "Integrated Electrochemical Aptasensor Array toward Monitoring Anticancer Drugs in Sweat". In: *Analytical Chemistry* 96.12 (2024), pp. 4997–5005.

[52] Xiaoyu Zhang et al. "Integrated aptasensor array for sweat drug analysis". In: *Analytical Chemistry* 94.22 (2022), pp. 7936–7943.

[53] Suresh Balakrishnama and Aravind Ganapathiraju. "Linear discriminant analysis-a brief tutorial". In: *Institute for Signal and information Processing* 18.1998 (1998), pp. 1–8.

[54] Annemarijn SM Steijlen et al. "Dual microfluidic sensor system for enriched electrochemical profiling and identification of illicit drugs on-site". In: *Analytical Chemistry* 96.1 (2023), pp. 590–598.

[55] Robin Van Echelpoel et al. "Unlocking the full potential of voltammetric data analysis: A novel peak recognition approach for (bio) analytical applications". In: *Talanta* 233 (2021), p. 122605.

[56] JC Alva-Ensastegui et al. "Determination of pKa values and deprotonation order of methotrexate using a combined experimental-theoretical study and binding constants of the methotrexate-Laponite complex at different pH values". In: *Journal of Photochemistry and Photobiology A: Chemistry* 449 (2024), p. 115406.

[57] Harker Mark and Clive R Harding. "Amino acid composition, including key derivatives of eccrine sweat: potential biomarkers of certain atopic skin conditions". In: *International journal of cosmetic science* 35.2 (2013), pp. 163–168.

[58] Lindsay B Baker and Anthony S Wolfe. "Physiological mechanisms determining eccrine sweat composition". In: *European journal of applied physiology* 120 (2020), pp. 719–752.